

RSC Advances



This is an *Accepted Manuscript*, which has been through the Royal Society of Chemistry peer review process and has been accepted for publication.

Accepted Manuscripts are published online shortly after acceptance, before technical editing, formatting and proof reading. Using this free service, authors can make their results available to the community, in citable form, before we publish the edited article. This *Accepted Manuscript* will be replaced by the edited, formatted and paginated article as soon as this is available.

You can find more information about *Accepted Manuscripts* in the [Information for Authors](#).

Please note that technical editing may introduce minor changes to the text and/or graphics, which may alter content. The journal's standard [Terms & Conditions](#) and the [Ethical guidelines](#) still apply. In no event shall the Royal Society of Chemistry be held responsible for any errors or omissions in this *Accepted Manuscript* or any consequences arising from the use of any information it contains.

Insight into Luminescent Bisazoaromatic *CNN* Pincer Palladacycle: Synthesis, Structure, Electrochemistry and Some Catalytic Applications in C–C Coupling†

Sima Roy, Shuvam Pramanik, Tapas Ghorui and Kausikisankar Pramanik*

Department of Chemistry, Inorganic Chemistry Section, Jadavpur University, Kolkata – 700032, India. E-mail: kpramanik@hotmail.com; Tel: +9133 2457 2781

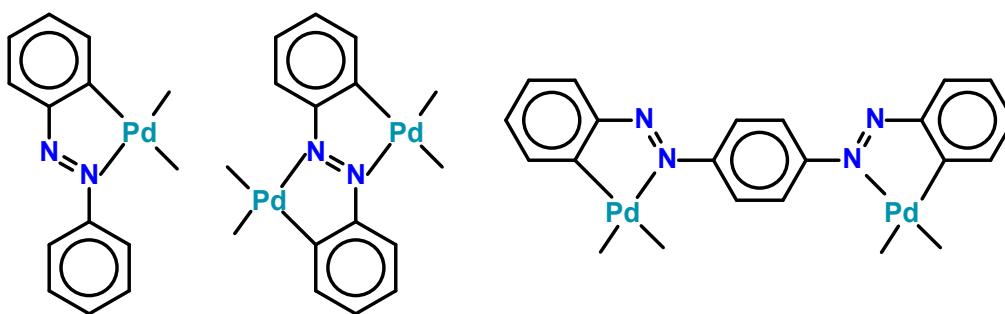
ABSTRACT

Chelating behavior of a potential flexidentate bisazoaromatic molecule 2-(phenylazo)azobenzene (PAAB) toward palladium have been examined. Activation of one instead of the two C(Ph)–H bonds of PAAB (HL) in due course of the metallation furnishes an exclusive unsymmetrical mode of ligation. Consequently, another member of the important class of *CNN* pincer palladacycles is achieved in almost quantitative yields. Crystallographic analysis authenticates the monoanionic terdentate ligation of the bisazoaromatic molecule and neutral $[Pd^{II}(L)X]$ ($X =$ acetate and halides) complexes with planar palladacycle and out-of-plane pendant phenyl ring. Unlike the N-donor pincers incorporating imine moieties, the introduction of two azo chromophores not only make the PAAB ligand significantly π -acidic but also modulates the FMOs in the palladacycles a lot. An appreciable lowering of ligand-centered (LC) π^* orbitals is apparent upon complexation which is in accordance with the electrochemical responses where large anodic shifts of LC LUMO and LUMO + 1 by 0.8–0.9 V have been noted. The significant modification of FMOs leads to interesting optoelectronic property in the palladacycles. The cyclopalladated compounds are luminescent in solution at room temperature. This property is plausibly a result of the LC emissive states (azo π^*). The optoelectronic features are interpreted by the Time-Dependant (TD) Density functional theory (DFT) and natural transition orbital (NTO) analyses. In addition, scrutiny of Suzuki-Miyaura and Heck-type reactions indicates that the pincer palladacycles may be employed in the development of useful catalysts for the C–C coupling reactions.

Introduction

After the discovery of a $[C,N]$ palladacycle *via* activation of *ortho* C–H bond of azobenzene by Cope and coworkers¹ in 1965, orthometallated palladium compounds have received increasing attention with azo, imine and other functionalities over the decades in coordination and organometallic chemistry.² Among azobenzene complexes, two types of coordination modes namely monocyclopalladated³ and doubly cyclopalladated⁴ species have been documented (Scheme 1). Recently, another form of doubly cyclopalladation has been reported with *p*-bisazobenzene (Scheme 1).⁵ Transition metal complexes with

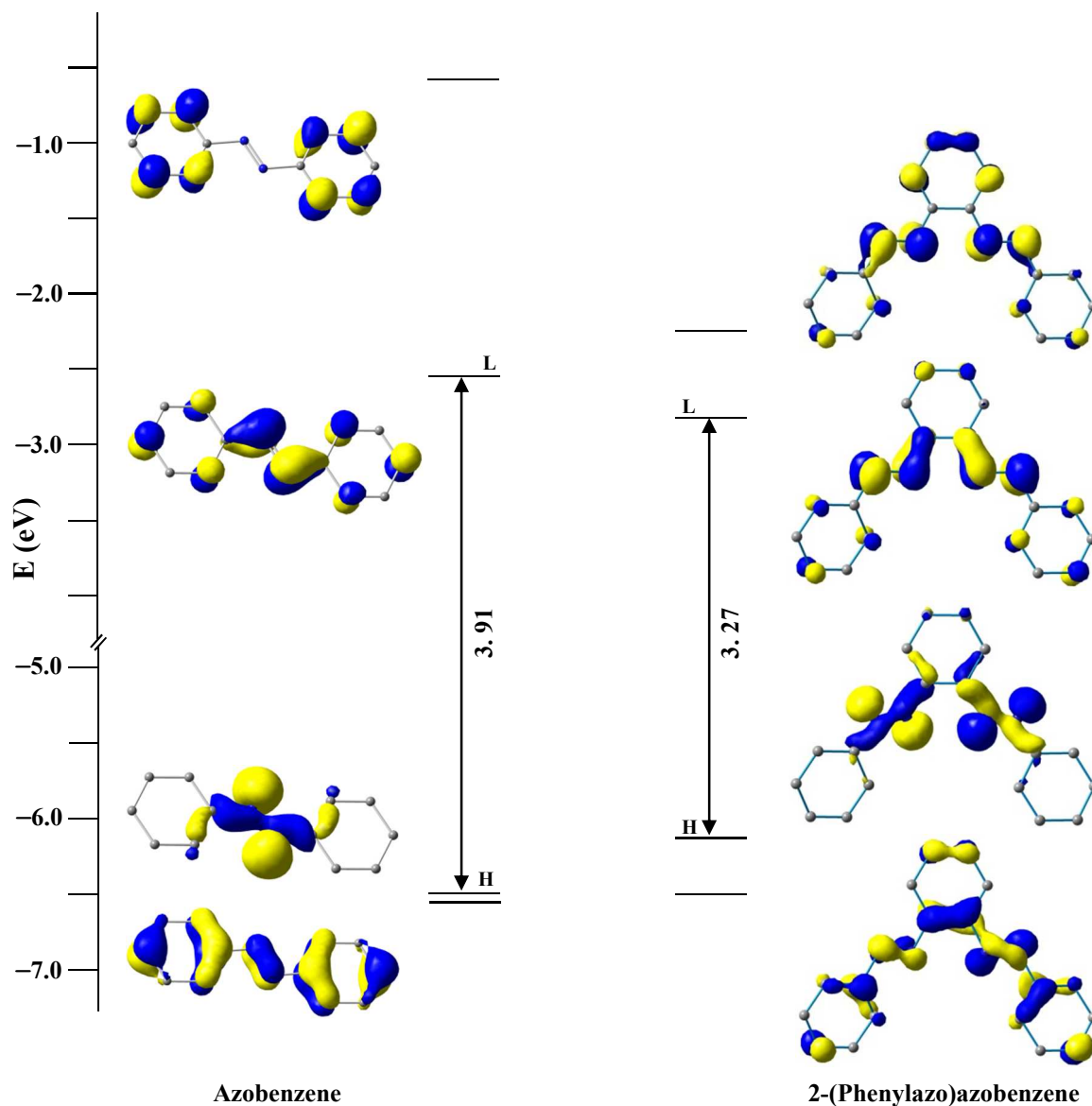
Scheme 1. Mono- and doubly cyclopalladation of azobenzene and *p*-bisazobenzene



azo chromophore have been found to display interesting physicochemical properties such as photoluminescence (PL), photoconductivity, photoisomerization in addition to electrochemical and catalytic activities.⁶ Notably, $[C,N]$ palladacycles reported so far contain single azo chromophore. Introduction of a higher homologue of azobenzene with multiple azo functionalities may appear as an attractive route to synthesize interesting azo compounds. We have employed a ligand incorporating two azo chromophores in conjugation with phenyl rings 2-(phenylazo)azobenzene (PAAB) (Scheme 2). A comparison of frontier molecular orbitals (FMOs) of PAAB with that of azobenzene signifies superior σ -donor as well as π -acceptor behavior of the former (Scheme 2). The reason behind the choice of such multidentate azoaromatic compound lies in its orthometallating nature and azo-based enhanced π -acceptor ability, which causes strong d-orbital splitting and leads to significant stabilization of lower valence states of the metal. The significant stabilization of ligand-centered (LC) virtual FMOs in the bisazoaromatic system relative to that of metal-centered (MC) level may offer an easy way to modify the optoelectronic properties of the palladacycles. The complexes display luminescence in fluid solution at room temperature. The reports on luminescent mononuclear nonporphyrin palladacycles at room temperature are sparse and they usually display luminescence only in a rigid matrix at 77 K.^{7,8} Recently, Che and coworkers reported the most luminescent Pd(II) complexes till date in fluid solution using tetradentate *ONCN* ligand.⁹ The lack of room temperature luminescence for cyclopalladated compounds

in solution is likely due to population of thermally accessible low-lying MC state ($4d_{x^2-y^2}$) which leads to effective non-radiative decay through severe excited-state structural distortion.¹⁰

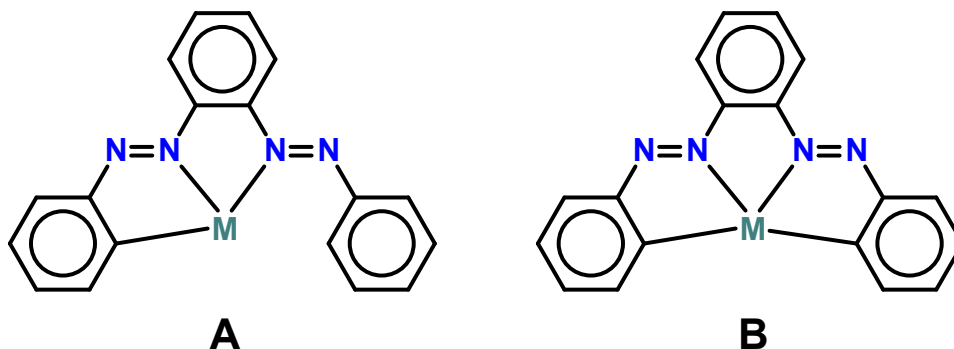
Scheme 2. Comparison of FMOs between azobenzene and 2-(phenylazo)azobenzene at B3LYP/(6-311+G(d,p) level



Though a report of isolation and in part characterization of the ligand has been previously documented,¹¹ we present a modified synthetic procedure with comprehensive characterization including crystal structure determination. We observe an exclusive pincer $C_{Ph}N_{azo}N_{azo}$ type ligation of PAAB toward Pd(II) (coordination mode A), nonetheless the free ligand possesses four potential donors following the activation of two C–H bonds (Scheme 3). Accordingly, the ligand provides another member of the

important class of unsymmetrical *CNN* pincer. The *CNN* pincer complexes incorporating Pd(II) are less common compared to that of Pt(II).^{7a,8e,12} Notably, pincer type palladacycles are one of the most well-

Scheme 3. Probable coordination modes of PAAB



known and scrutinized classes of orthometallated compounds.¹³ These attractive classes of non-phosphine palladacycles disclose a challenge to chemists not only in terms of their synthesis but also in terms of their structure, design, and the mode of coordination of the ligand to the metal. Significantly, unlike conjugated aromatic polyimine molecules, the polyazo ligands are sparse in the pincer chemistry and there are only two recent reports¹⁴ of bisazoaromatic ligands *viz.* 3-(phenylazo)azobenzene and 2,6-bis(phenylazo)pyridine with Rh(III) and Fe(II) respectively. It is worth mentioning that the variation of coordinating atoms in the anionic six-electron donor ligand may alter the nature of the metal center radically and make the palladacycles useful for much wider application in the organic synthesis and catalysis.¹⁵ In this context, deployment of superior π -accepting pincers are most enviable since the majority of catalytic cycles of Pd-catalyzed reactions are generally based on Pd^{II}/Pd⁰ shuttles.¹⁶ In this work, we report the high-yield synthesis and characterization of a new set of unsymmetrical *CNN* pincer palladacycles with 2-(phenylazo)azobenzene, as well as the discussion and rationalization of their structural and optoelectronic properties. Presence of low-lying LC virtual orbitals is appraised by means of electrochemical study (cyclic voltammetry). The experimental results are complemented by theoretical calculations in order to explain the nature of the electronic transitions in the palladacycles. Preliminary catalytic activity of the non-phosphine Pd(II) complexes has been explored toward C–C coupling reaction.

Results And Discussion

Synthesis, Characterization and Electrochemical study

The PAAB ligand was synthesized by Baeyer-Mills coupling reaction¹⁷ of 2-(amino)azobenzene with nitrosobenzene in glacial acetic acid at elevated temperature followed by the extraction with *n*-hexane. The reaction of Pd(OAc)₂ and PAAB in glacial acetic acid afforded [Pd(L)OAc] **1** in almost quantitative yield. The chloro derivative [Pd(L)Cl] **2** was obtained from K₂[PdCl₄] under similar reaction conditions in near stoichiometric yield. The ligand furnishes unsymmetrical terdentate *CNN* mode of coordination in the palladacycles following the activation of one C(Ph)–H bond despite of the presence of two such C–H bonds in the free ligand. Coordination mode A is favored over coordination mode B plausibly due to get rid of the structural strain within the rigid PAAB skeleton. The anionic six-electron donor PAAB furnishes two contiguous five-membered chelates and provides robust metal-organic conjugates, which limit their dissociation from the metal center. The other halo derivatives [Pd(L)Br] **3** and [Pd(L)I] **4** are obtained by substituting the OAc[−] of **1** with the respective excess of X[−] (X = Br, I) in acetone. All the complexes are soluble both in polar and nonpolar solvents such as toluene, dichloromethane, acetonitrile, ethanol, ether and furnishing a red solution. The acetato complex was obtained as H-bonded dimer, where the free O atoms of acetato groups are linked with one water molecule *via* H bonding. The presence of water of hydration was corroborated with thermogravimetric analysis (TGA). Thermogram (ESI, Fig. S1†) shows two decomposition steps within the temperature range 40–300 °C. The first step of decomposition, within the temperature range 40–150 °C, corresponds to the loss of water molecule of hydration with a mass loss of 2.2% (calcd. 2.0%). The second step (150–300 °C) corresponds to the removal of the acetate group with a mass loss of 12.7% (calcd. 13.1%). Sharp vibrations around 1486–1439 cm^{−1} in the infrared spectra of the free ligand were assigned to the ν_{N=N} (ESI, Fig. S2†). The observed lowering of ν_{N=N} values in complexes (1445–1430 cm^{−1}) as compared to that of free ligand is consistent with the Pd(II) → π*(azo) back-bonding. An electrospray ionization (ESI) mass spectrum (MS) of the ligand in acetonitrile displays a peak at *m/z* 287 amu for [L + H]⁺ (ESI, Fig. S3†). The analogous spectra of complexes show the peaks for [M – X]⁺ and [2M – X]⁺ with the expected isotopic distribution pattern (ESI, Fig. S4†), indicating their substantial stability in solution. The NMR spectra of ligand and complexes are presented in ESI (Fig. S5–S6†).

The redox behavior of the uncoordinated ligand and the cyclopalladated compounds has been scrutinized by cyclic voltammetry; the data collected in Table 1. The free ligand exhibits two successive one-electron quasi-reversible reductive responses, at −1.21 and −1.51 V (*vs* Ag/AgCl) (Fig. 1), indicating the chronological filling of π* orbitals. The facile reductive nature of PAAB is consistent with its superior π-acceptor ability. A significant anodic shift of these redox couples, by ~0.9 and ~0.8 V respectively, was observed upon palladation (Fig. 1). The reductive responses near −0.25 and −0.75 V *vs* Ag/AgCl may be

attributed to the azo reductions in the complexes and this trend can be ascribed to remarkable stabilization of ligand-centered LUMO and LUMO + 1 in presence of electro-positive metal center.

Table 1 Electrochemical Data^a

Compound	$E_{1/2}/V$ ($\Delta E_p/mV$)
PAAB	-1.21(160), -1.51(160)
[Pd(L)(OAc)] 1	-0.30(81), -0.76(76)
[Pd(L)Cl] 2	-0.28(80), -0.73(76)
[Pd(L)Br] 3	-0.26(82), -0.74(78)
[Pd(L)I] 4	-0.26(82), -0.73(77)

^a Solute concentration $\approx 10^{-3}$ mol dm⁻³; scan rate, 50 mV s⁻¹; $E_{1/2} = 0.5(E_{pa} - E_{pc})$, where E_{pa} and E_{pc} are the anodic and cathodic peak potentials, respectively; $\Delta E_p = E_{pa} - E_{pc}$.

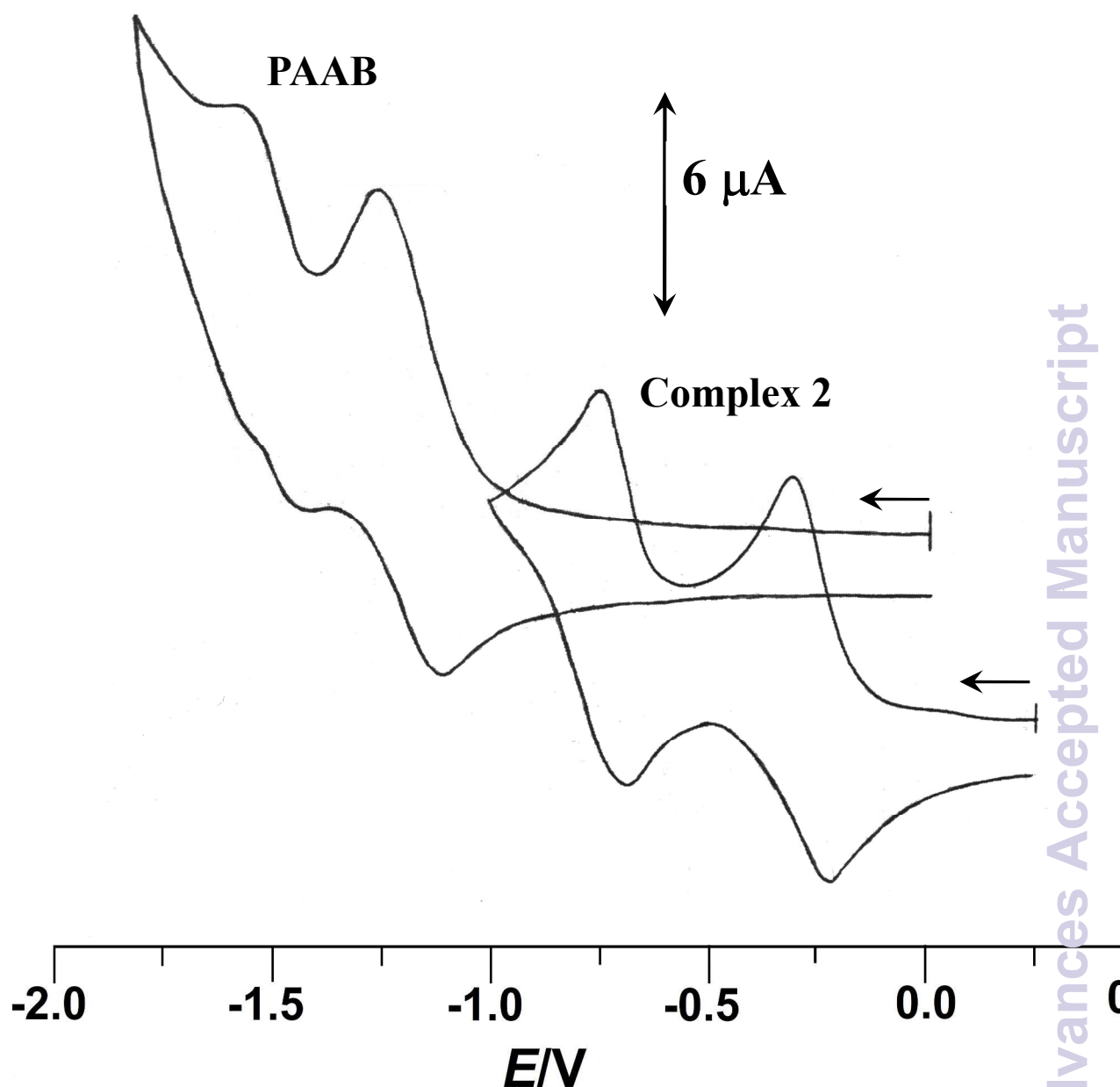


Fig. 1 Voltammogram of PAAB and **2** in acetonitrile at 50 mV s^{-1}

To gain insight into the nature of the redox orbitals, we have performed DFT calculation of the free ligand and complexes. The observed redox responses nicely substantiated with the theoretical study. Illustrations of the selected FMOs of the complexes are presented in Fig. 2. Calculation indicates that LUMO and LUMO + 1 of PAAB encompass exclusively the azo as well as phenyl moieties and remain symmetric along the C_2 axis. A sizeable stabilization of both LUMO and LUMO + 1 by ~ 0.60 and ~ 0.75 eV respectively upon complexation has been computed (ESI, Table S1–S5†). In these complexes, a slight polarization between the coordinated and pendant phenyl rings has been observed for these virtual orbitals. The energies of these FMOs in the palladacycles remain almost insensitive with the nature of

coligands, excluding their involvement in the redox processes. The components of LUMO and LUMO + 1 of all the complexes are essentially similar in nature and comprise exclusively azo- π^* (50%) and phenyl- π^* (50%) of coordinated bisazoaromatic ligand with practically no participation of metal orbitals (ESI, Table S2–S5†). It is very likely that these electrochemical processes correspond to the reduction of the bisazoaromatic system, generating the metal-stabilized azo anion radicals (eq 1 and eq 2). Redox noninnocence behavior of the azo ligands is well documented in the literature.¹⁸

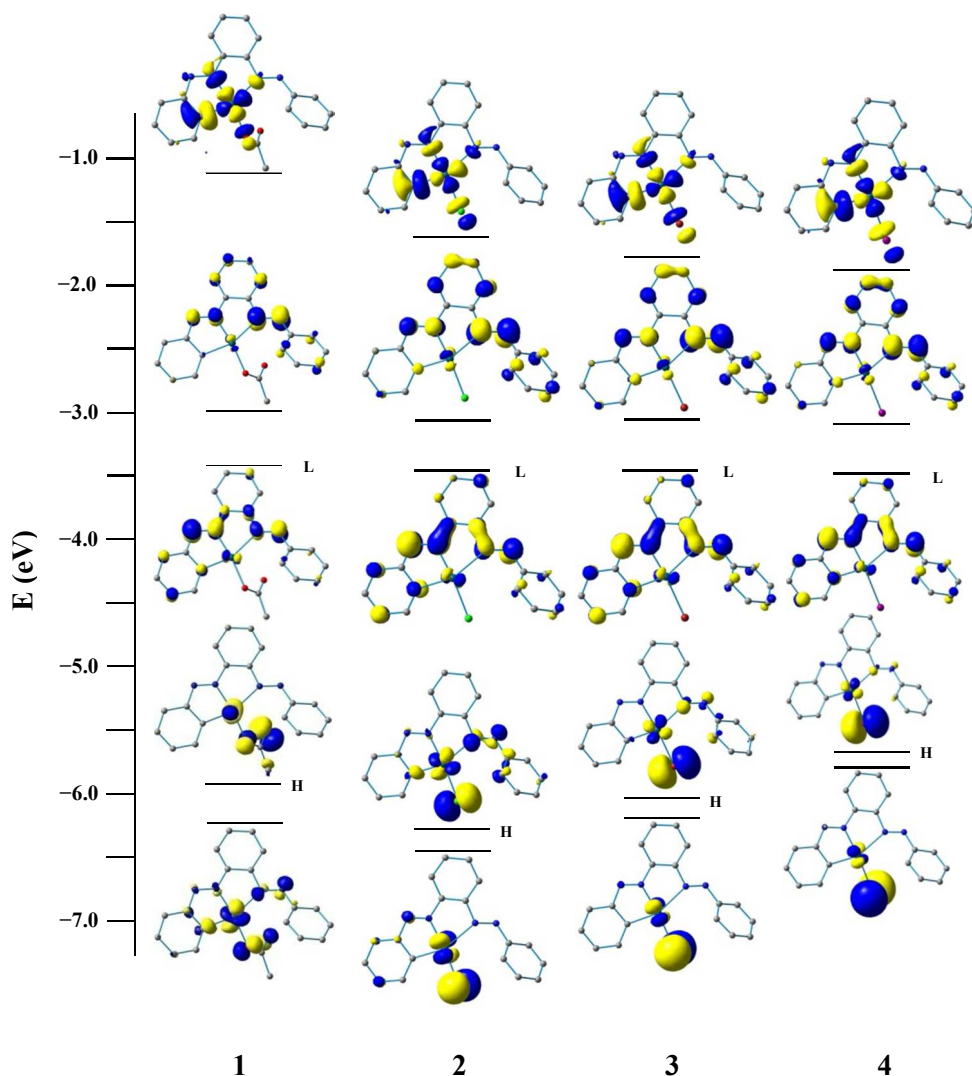
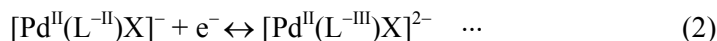
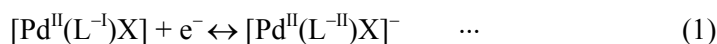


Fig. 2 Isodensity surface plots of some selected FMOs (HOMO – 1 to LUMO + 2) for the complexes **1**, **2**, **3** and **4** at their optimized S_0 geometry in gas phase (Isodensity value 0.05 e Bohr^{-3}).

Crystal Structures

The structures of the free ligand and all four complexes have been authenticated by single-crystal X-ray diffraction. Crystallographic details are given in ESI (Table S6†), significant metrical parameters in Table 2. Rod-shaped crystals suitable for X-ray crystallography of the free ligand have been grown by slow evaporation of hexane solution of the compound. Fig. 3 shows the ORTEP and atom numbering scheme of PAAB. The X-ray crystallographic analysis reveals a symmetrical (C_2) and almost planar structure ($md = 0.165 \text{ \AA}$), with practically identical d_{N-N} values of 1.244(1) and 1.243(1) \AA for two azo groups, respectively. Two phenylazo groups are lying opposite to each other with respect to the plane passing through the central benzene ring (inset of Fig. 3).

Table 2 Selected Metrical Parameters for PAAB, **1**, **2**, **3** and **4**

Bond Parameter	PAAB	1	2	3	4
Pd1–C1		1.974(2)	1.971(3)	1.978(3)	1.984(5)
Pd1–N2		1.945(2)	1.961(2)	1.971(2)	1.973(4)
Pd1–N3		2.182(2)	2.229(2)	2.227(2)	2.207(4)
Pd1–O1		2.053(2)			
Pd1–Cl1			2.289(1)		
Pd1–Br1				2.412(1)	
Pd1–I1					2.590(1)
N1–N2	1.244(1)	1.274(2)	1.282(3)	1.280(3)	1.272(5)
N3–N4	1.243(1)	1.258(3)	1.242(3)	1.252(3)	1.258(5)
C1–Pd1–N2		79.27(9)	79.49(10)	79.70(10)	79.39(17)
N2–Pd1–N3		80.69(7)	78.90(9)	78.70(9)	78.75(14)
O1S...O2A (H1SB...O2A)		2.868 (2.036)			
O1S...O4A (H1SB...O4A)		2.869 (2.086)			

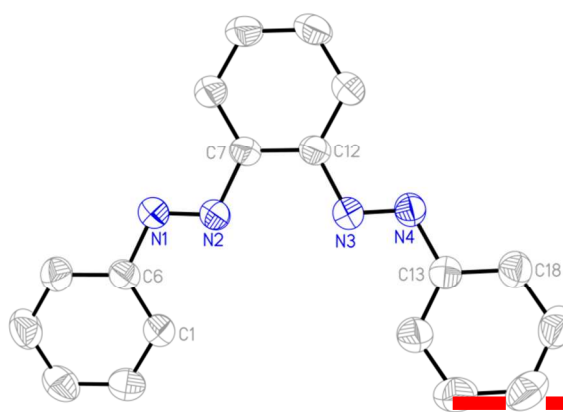


Fig. 3 ORTEP of PAAB with ellipsoids at the 50% probability level. Hydrogen atoms are omitted for clarity. Inset: Molecular view along the plane passing through the central benzene ring.

Single crystals of complexes **1–4** suitable for X-ray diffraction analysis were grown by slow diffusion of their respective toluene solution into hexane solvent. The ORTEP and atom-numbering scheme are shown in Fig. 4. The bis azo ligand acts as monoanionic tridentate donor toward Pd(II) using one C_{Ph} and two N_{azo} atoms with the formation of two contiguous five-membered chelates, albeit it

possesses four potential donor atoms; furnishing an unsymmetrical coordination mode. The coordination geometry of all the complexes is described as a square planar with two dissimilar Pd–N(azo) bond lengths differ by ~ 0.25 Å. The N_{azo} atom closer to orthometallated C_{ph} forms a stronger bond with the metal relative to the other N_{azo} atom. The appreciable difference in Pd– N_{azo} bond lengths is reflected in the corresponding $d_{\text{N-N}}$ distances. The lengthening of N1–N2 as compared to N3–N4 bonds by ~ 0.03 Å is in accordance with the greater amount of Pd(d) \rightarrow azo(π^*) back donation in the former azo linkage. A systematic variation in the Pd–N2 bond was observed in the four complexes with the shortest length in **1** and the longest in **4**. This observation is in accordance with the trans effect order: $\text{I}^- > \text{Br}^- > \text{Cl}^- > \text{OAc}^-$.

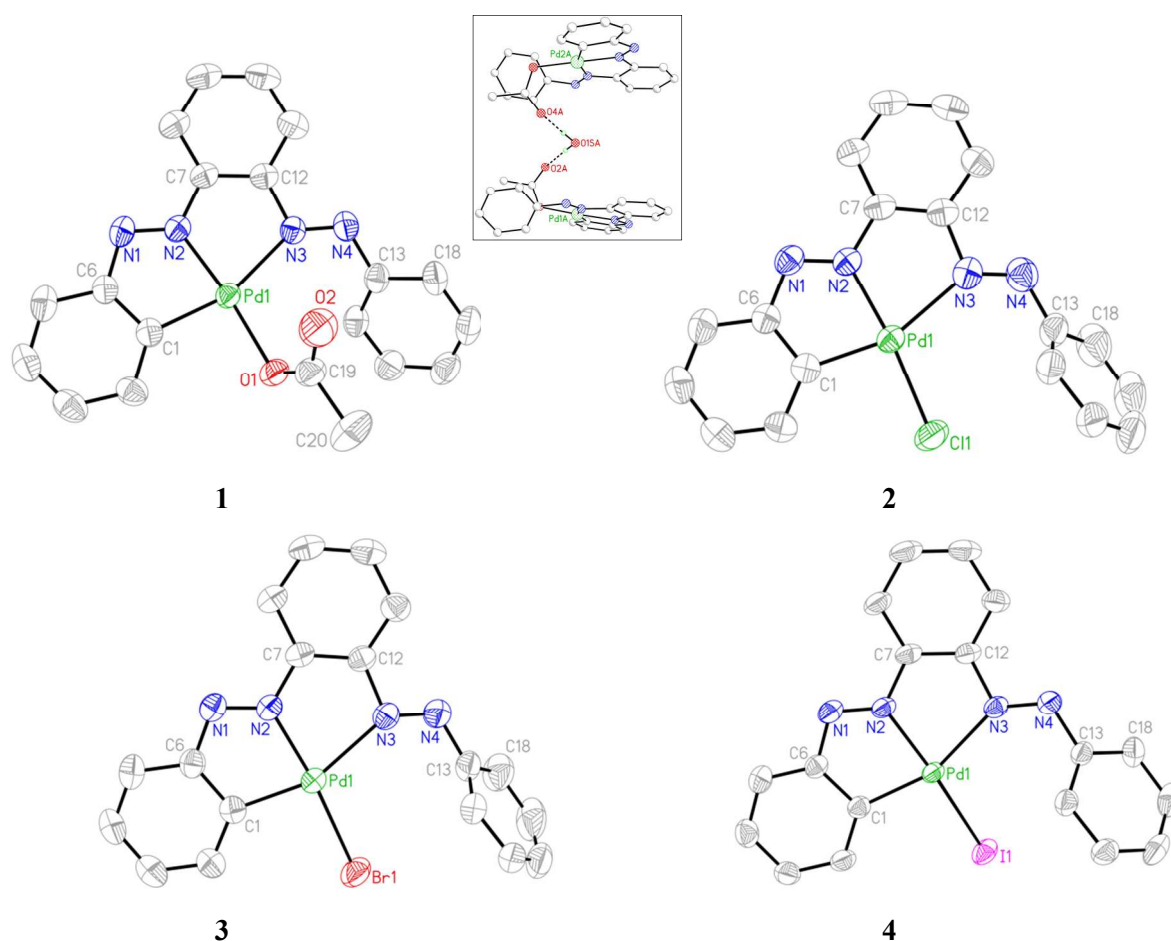


Fig. 4 ORTEP of **1–4** with ellipsoids at the 50% probability level. Hydrogen atoms are omitted for clarity. Inset: H-bonding interaction in acetato complex.

The Pd1–N3 bond length remains almost unaltered in the halo compounds while a slight decrease of ~ 0.04 Å in **1** occurs possibly due to less steric crowding. The pendant phenyl rings (C13–C18) do not lie on the molecular plane in the complexes and makes an angle varying in the range 41 – 68° with the rest. Crystallographic analysis reveals that the two acetato complexes are joined *via* intervening water

molecule with strong H-bonding ($O_{\text{acetato}} \cdots O_{\text{water}}$ 2.87(1) Å) as shown in the inset of Fig. 4. The chelate bite angle C1–Pd1–N2 is marginally larger than that of N2–Pd1–N3 by $\sim 1^\circ$.

Ground State Geometries and Frontier Molecular Orbital Compositions

All the complexes are diamagnetic at room temperature indicating their singlet ground state. The geometry optimizations of the complexes were performed using their crystallographic coordinates at (R)B3LYP levels in gas phase in their singlet spin state without any ligand simplification. The optimized geometries of the synthesized complexes and the significant metrical parameters are given in ESI (Fig. S7–S8† and Table S7† respectively). The optimized structural parameters of **1**, **2**, **3** and **4** are in general agreement with the experimental values and the slight discrepancy arises due to the crystal lattice distortion existing in real molecules. The calculated N–N(azo) distance of the free ligand ($d_{\text{N–N}}$ 1.253 Å) is found to be shorter, as compared to their coordinated forms (average $d_{\text{N–N}}$ 1.276 and 1.263 Å, respectively), indicating reasonable population of ligand π^* in complexes. Isodensity plots of some selected FMOs of the Pd(II) complexes and energy levels (H – 1 to L + 2) are depicted in Fig. 2. The partial frontier molecular orbital compositions of the PAAB ligand and the Pd(II) complexes along with the HOMO–LUMO energy gap, are listed in ESI (Table S1–S5†).

In the ground state, the HOMO of **1** mainly consists of 2p(OAc) with little $4d_z^2$ (Pd) character, while that of **2** is constituted largely of 3p(Cl) with minor participation of π (Ph) and π (azo). The more stabilized HOMO – 1 in both the complexes are constituted of comparable metal participation ($\sim 25\%$), whereas the involvement of the respective coligand OAc/Cl differs appreciably. The HOMO and HOMO – 1 are mostly 4p(Br)/5p(I) coligand character for **3** and **4**. The LUMO and LUMO + 1 are essentially similar in all four complexes and composed of $\sim 50\%$ π^* (azo) and $\sim 50\%$ π^* (Ph) of the PAAB ligand. These two FMOs are substantially stabilized upon complexation. It is worth noting that the LUMO + 2 in these complexes are basically analogous in nature and alike to $4d_{x^2-y^2}$ of Pd ($\sim 45\%$) with substantial contribution of π^* (Ph) ($\sim 35\%$). Computation, therefore, reveals that LUMO and LUMO + 1 (LC states) are appreciably stabilized relative to the LUMO + 2 (MC level) by 1.85 and 1.45 eV, respectively.

Photophysical Studies

a. UV-Vis Absorption Spectra Electronic spectra of compounds **2** and **4** were recorded in dichloromethane at room temperature and are depicted in Fig. 5 along with their respective theoretical spectra and that of compounds **1**, **3** and PAAB are shown in ESI (Fig. S9†). More structured profile observed for palladacycles may result from the increased electronic asymmetry caused by the presence of the electron-accepting PAAB ligand. Multiple transitions are the characteristics of the spectra for these complexes (Table 3) and the excitations are attributed primarily to the charge-transfer transitions within the tri-coordinated bisazoaromatic ligand with varying amounts of anionic coligand-p orbital and metal-d

orbital participation. To gain deeper insight into the electronic properties of the transitions involved in the optical absorption processes, we investigated all the synthesized complexes by means of time-dependent density functional theory (TD-DFT) in CH_2Cl_2 solvent using CPCM model. The most relevant transitions involved, along with their energy, character, oscillator strengths of all the compounds, are listed in ESI (Table S8–S11†). In order to analyze the nature of absorption, we performed an NTO analysis based on the calculated transition density matrices.¹⁹ This method offers the most compact representation of the transition density between the ground and excited states in terms of an expansion into single-particle transitions (hole and electron states for each given excitation). Here we refer to the unoccupied and occupied NTOs as “electron” and “hole” transition orbitals. The NTOs for **1** are illustrated in Fig. 6 and that of **2**, **3** and **4** are given in ESI (Fig. S10–S12†). Based on TD-DFT NTO analysis for **1**, lower energy transition around 545 nm is computed at 580 nm (2.1354 eV, $f = 0.0730$) and 504 nm (2.4585 eV, $f = 0.0459$) as the $4d_{zx}(\text{Pd}) + 2p(\text{OAc}) + \pi(\text{Ph}) \rightarrow \pi^*(\text{azo} + \text{Ph})$ $^1\text{MLCT}/^1\text{LLCT}/^1\text{ILCT}$ transition. The

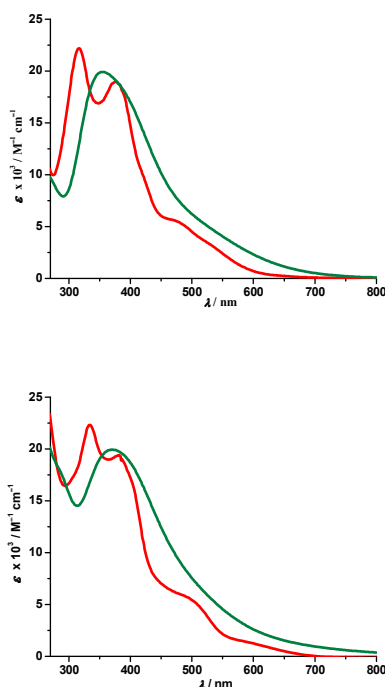


Fig. 5 Experimental (red) and theoretical (green) absorption spectra of **2** (top) and **4** (bottom)

transition near 475 nm (2.6842 eV, $f = 0.0673$, $\lambda_{\text{theo}} = 462$ nm) is computed as the $2p(\text{OAc}) + \pi(\text{Ph}) + 4d_{xy}(\text{Pd}) \rightarrow \pi^*(\text{azo} + \text{Ph})$ $^1\text{LLCT}/^1\text{ILCT}/^1\text{MLCT}$ transitions. For **2**, lower energy transitions around 530 nm and 480 nm are computed at 523 nm (2.3803 eV, $f = 0.0700$) and 488 nm (2.5421 eV, $f = 0.0669$) and both are attributed to the $4d_{zx}(\text{Pd}) + 3p(\text{Cl}) \rightarrow \pi^*(\text{azo} + \text{Ph})$ $^1\text{MLCT}/^1\text{LLCT}$ transition. For **3**, the lower energy transition around 560 nm is computed at 590 nm (2.1002 eV, $f = 0.0380$) as $4p(\text{Br}) + 4d_{xy}(\text{Pd}) +$

$\pi(\text{azo}) \rightarrow \pi^*(\text{azo} + \text{Ph})$ $^1\text{LLCT}$ admixed with some $^1\text{MLCT}/^1\text{ILCT}$ character and at 524 nm (2.3660 eV, $f = 0.0353$) as $4d_z^2(\text{Pd}) \rightarrow \pi^*(\text{azo} + \text{Ph})$ $^1\text{MLCT}$ transition. The shoulder near 490 nm is calculated at 503 nm (2.4642 eV, $f = 0.0685$) as $4p(\text{Br}) + 4d_z^2(\text{Pd}) + \pi(\text{Ph}) \rightarrow \pi^*(\text{azo} + \text{Ph})$ $^1\text{LLCT}/^1\text{MLCT}/^1\text{ILCT}$ transition. For **4**, lowest energy transition around 600 nm is computed at 653 nm (1.8970 eV, $f = 0.0257$)

Table 3 UV-vis and luminescence spectral data^a for **1**, **2**, **3** and **4** in dichloromethane at room temperature

Compound	$\lambda_{\text{max}}[\text{nm}]$ (ϵ [$\text{M}^{-1}\text{cm}^{-1}$])	λ_{em} (nm)	τ (ns)	Φ ($\times 10^{-3}$)	k_r , s^{-1} ($\times 10^5$)	k_{nr} , s^{-1} ($\times 10^8$)
PAAB	306 (26500), 343 ^b (19900), 446 ^b (1000)	384	7.06	4.507	6.384	1.410
1	316 (23700), 375 (20000), 475 ^b (5700), 545 ^b (2900)	369	9.52	4.531	4.759	1.046
2	323 (22300), 381 (19000), 480 ^b (5600), 530 ^b (3200)	352	9.13	3.018	3.306	1.092
3	318 (25500), 377 (21000), 490 ^b (6000), 560 ^b (2500)	352	8.71	7.546	8.664	1.139
4	334 (22400), 382 (19400), 500 ^b (5500), 600 ^b (1300)	352	9.23	9.358	10.139	1.073

^a The compounds PAAB, **1**, **2**, **3** and **4** are excited at 324 nm. ^b Shoulder.

as predominantly $5p(\text{I}) \rightarrow \pi^*(\text{azo} + \text{Ph})$ $^1\text{LLCT}$ transition. The next lower energy transition near 500 nm is computed at 507 nm (2.4414 eV, $f = 0.0347$) and 503 nm (2.4631 eV, $f = 0.0921$). The first one can be exclusively ascribed to $4d_z^2(\text{Pd}) \rightarrow \pi^*(\text{azo} + \text{Ph})$ $^1\text{MLCT}$ transition and the latter one is assigned to $\pi(\text{Ph}) + 4d_{zx}(\text{Pd}) \rightarrow \pi^*(\text{azo} + \text{Ph})$ $^1\text{ILCT}/^1\text{MLCT}$ transition. In the UV region two distinct excitations near 380 and 325 nm are observed. The former excitation can be assigned exclusively as $\pi(\text{Ph}) \rightarrow \pi^*(\text{azo} + \text{Ph})$ $^1\text{ILCT}$ transition for **1** while incorporation of some $4d_z^2(\text{Pd}) \rightarrow \pi^*(\text{azo} + \text{Ph})$ $^1\text{MLCT}$ character is found in the halo analogues **2–4**. In contrast, higher energy UV absorption at 316 nm of **1** is described mostly as $\pi(\text{Ph}) \rightarrow \pi^*(\text{azo})$ $^1\text{ILCT}$ transition mixed with small $^1\text{MLCT}$ nature. For **2**, the corresponding peak at 323 nm is assigned as $\pi(\text{azo} + \text{Ph}) + 4d_z^2(\text{Pd}) \rightarrow \pi^*(\text{azo} + \text{Ph})$ $^1\text{ILCT}$ transition admixed with small $^1\text{MLCT}$ character. The analogous transition at 318 nm (3.7788 eV, $f = 0.0296$, $\lambda_{\text{theo}} = 312$ nm) in **3** is computed as $\pi(\text{Ph} + \text{azo}) + 4p(\text{Br}) \rightarrow \pi^*(\text{azo} + \text{Ph})$ and can be attributed to $^1\text{ILCT}/^1\text{LLCT}$. In **4**, the related band ($\lambda_{\text{exp}} = 334$ nm, $\lambda_{\text{theo}} = 348$ nm) can be ascribed largely as $\pi(\text{Ph}) \rightarrow \pi^*(\text{azo} + \text{Ph})$ $^1\text{ILCT}$ transition admixed with some $^1\text{LLCT}$ character originated from $5p(\text{I})$.

The lowest energy transitions in the complexes are affected largely by the nature of anionic coligand. Each of these excitations originates from energetically dissimilar occupied orbitals *i.e.*, exclusive $5p$ orbital of iodine in **4**, while the involvement of metal t_2 becomes the dominating feature on

going from **3** to **1**. In contrast, almost similar unoccupied orbitals are found in all complexes and composed of mainly azo- π^* admixed with little phenyl- π^* . The bathochromic shift of longest wavelength transition from **1** to **4** is associated with the increasing order of polarizability of the anionic coligand. The

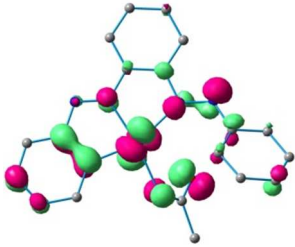
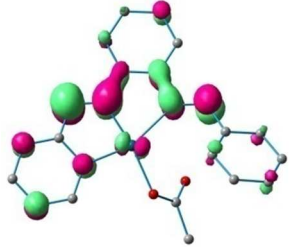
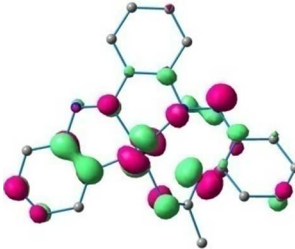
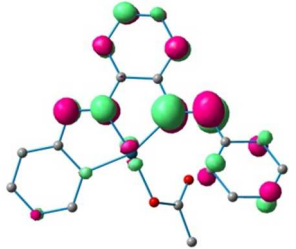
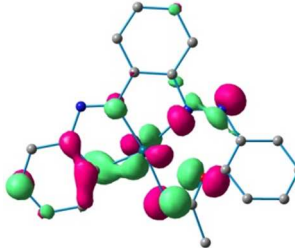
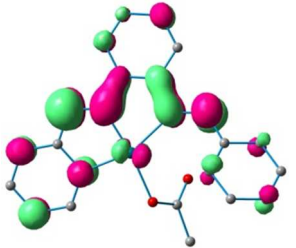
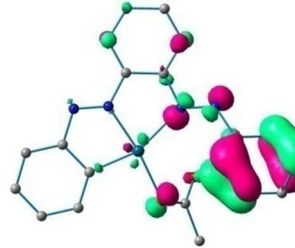
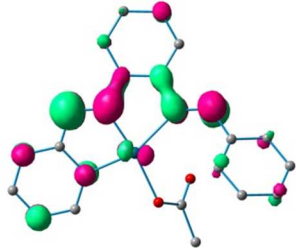
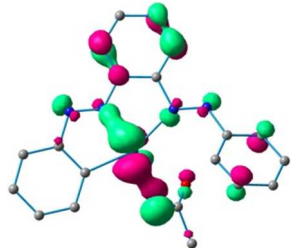
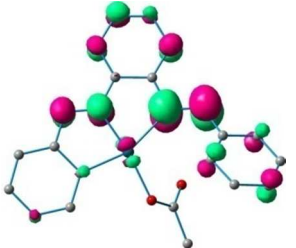
Complex			Hole	Electron
1	545 nm	S_2 w = 0.83 2.1354 (0.0730) 580.62 nm		
		MLCT/LLCT/ILCT $4d_{zx}(\text{Pd}) + \pi(\text{Ph}) + 2p(\text{OAc}) \rightarrow \pi^*(\text{azo} + \text{Ph})$		
		S_3 w = 0.51 2.4585 (0.0459) 504.31 nm		
		MLCT/LLCT/ILCT $4d_{zx}(\text{Pd}) + \pi(\text{Ph}) + 2p(\text{OAc}) \rightarrow \pi^*(\text{azo} + \text{Ph})$		
	475 nm	S_5 w = 0.57 2.6842 (0.0673) 461.90 nm		
	LLCT/ILCT/MLCT $\pi(\text{Ph}) + 2p(\text{OAc}) + 4d_{xy}(\text{Pd}) \rightarrow \pi^*(\text{azo} + \text{Ph})$			
375 nm	S_{13} w = 0.33 3.2966 (0.1139) 376.10 nm			
	ILCT $\pi(\text{Ph}) \rightarrow \pi^*(\text{azo} + \text{Ph})$			
316 nm	S_{20} w = 0.58 3.8130 (0.1829) 325.16 nm			
	ILCT/MLCT $\pi(\text{Ph}) + 4d_{yz}(\text{Pd}) \rightarrow \pi^*(\text{azo} + \text{Ph})$			

Fig. 6 Natural transition orbitals (NTOs) for complex **1** illustrating the nature of singlet excited states in the absorption bands in the range 250–700 nm. For each state, the respective number of the state, transition energy (eV), and the oscillator strength (in parentheses) are listed. Shown are only occupied (holes) and unoccupied (electrons) NTO pairs that contribute more than 25% to each excited state

major features in the 300–400 nm region in all the complexes can be attributed largely due to π – π^* within the terdentate ligand.

b. Luminescence Spectra The complexes exhibit broad luminescent maxima near 355 nm (Fig. 7) and these remain unaffected with the energy of excitation wavelengths. Time-resolved fluorescent spectra were recorded to understand the decay process and the emissive nature of the compounds (Fig. S13†, ESI). These are found to be moderate emitters (quantum yields (Φ) = 3.0 – 9.0×10^{-3}). The luminescence spectrum and time-resolved fluorescence decay plot of PAAB are depicted in ESI (Fig. S14†). Table 3 summarizes the emission maxima (λ_{em}), quantum yield (Φ), lifetime (τ), radiative (k_r) and nonradiative (k_{nr}) decay rate constants.

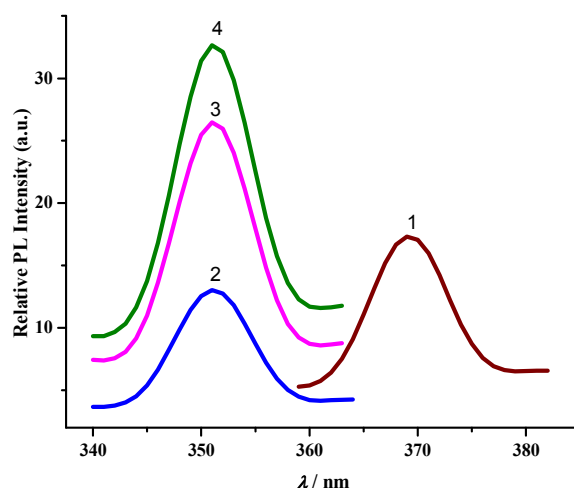


Fig. 7 Luminescence spectra of complexes.

All *CNV* pincer complexes in this account are emissive in solution at room temperature which is an uncommon phenomenon for Pd(II) compounds.⁷ This is due to the presence of thermal accessible metal-centred (MC) excited states, the geometry of which is strongly distorted with respect to that of the ground state, leading to the rapid deactivation of the excited luminescent state.¹⁰ The emission spectra of **1–4** are very similar and comparable to the spectrum of free ligand. In order to analyze the nature of emission, NTO analysis was performed based on the calculated transition density matrices in their singlet states. The NTOs are illustrated in Fig. 8. The broad luminescent band of the **1** in the experimental spectrum at 360 nm is computed at 356 nm (3.4853 eV, $f = 0.1492$) with significant transition having $\pi^*(azo + Ph) \rightarrow 2p(OAc) + \pi(Ph) + d_{yz}(Pd)$ and attributed to ${}^1ILCT/{}^1LLCT/{}^1LMCT$. The experimental emission spectrum ($\lambda_{em} = 352$ nm) of **2** is computed at 352 nm (3.5172 eV, $f = 0.0662$) and tentatively assigned to as $\pi^*(azo + Ph) \rightarrow \pi(Ph) + 3p(Cl)$ ${}^1ILCT/{}^1LLCT$ transition. The emission spectrum ($\lambda_{em} = 352$

nm) of **3** is computed at 348 nm (3.5598 eV, $f = 0.0553$) and can be ascribed to as $\pi^*(\text{azo}) \rightarrow \pi(\text{Ph}) + 4p(\text{Br})$ $^1\text{ILCT}/^1\text{ILCT}$ transition. Similarly, the observed band at 352 nm for **4** is computed at 348 nm (3.5619 eV, $f = 0.2726$) and can be tentatively assigned to as mostly $\pi^*(\text{azo}) \rightarrow \pi(\text{Ph}) + 5p(\text{I})$ $^1\text{ILCT}/^1\text{LLCT}$ admixed with $\pi^*(\text{azo}) \rightarrow d_{yz}(\text{Pd})$ $^1\text{LMCT}$ transition. The photoluminescence property mainly originates from singlet state charge transfer transitions revealing the ligand-centered ^1IL nature of the emissive state for all complexes. Our investigation has shown that the nature of the luminescent occupied (hole) transition orbitals of **1–4** and PAAB remains virtually similar and emerged as conjugated π^* orbital encompassed over both the azo chromophores (Fig. 8). The luminescent unoccupied (electron) transition orbital appears exclusively as $\pi(\text{Ph})$ in the free ligand while that in the palladacycles is dependent upon the nature of anionic coligands. The corresponding orbital appears as the

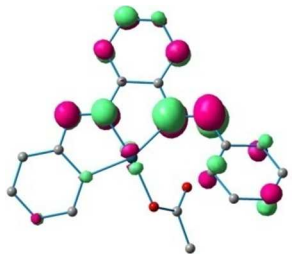
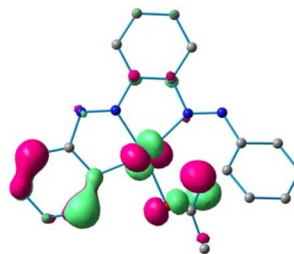
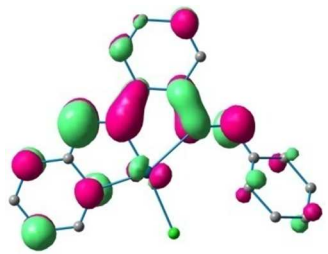
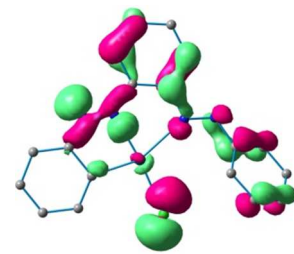
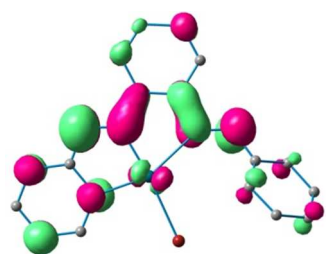
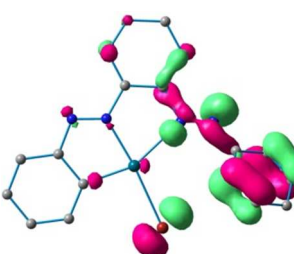
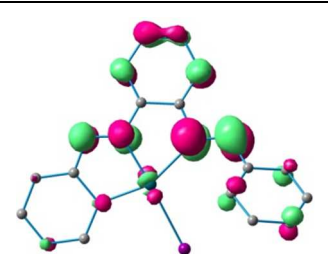
Complex			Hole	Electron
1	360 nm	S_{15} $w = 0.43$ 3.4853 (0.1492) 355.73 LMCT/ILCT $\pi^*(\text{azo} + \text{Ph}) \rightarrow$ $2p(\text{O}_{\text{OAc}}) + \pi(\text{Ph})$ $+ d_{yz}(\text{Pd})$		
2	352 nm	S_{14} $w = 0.33$ 3.5172 (0.0662) 352.51 LLCT $\pi^*(\text{azo} + \text{Ph}) \rightarrow$ $3p(\text{Cl}) + \pi(\text{Ph})$		
3	352 nm	S_{17} $w = 0.59$ 3.5598 (0.0553) 348.29 LLCT/ILCT $\pi^*(\text{azo}) \rightarrow \pi(\text{Ph})$ $+ 4p(\text{Br})$		
4	352 nm	S_{20} $w = 0.31$ 3.5619 (0.2726) 348.08 LLCT/LMCT $\pi^*(\text{azo}) \rightarrow \pi(\text{Ph})$ $+ 5p(\text{I}) + d_{yz}(\text{Pd})$		

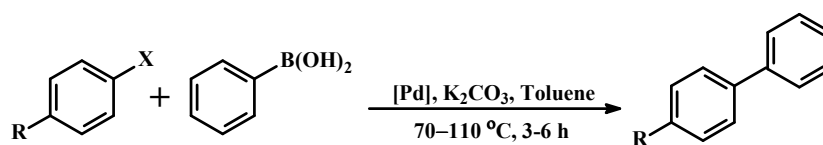
Fig. 8 Natural transition orbitals (NTOs) for the complexes **1**, **2**, **3** and **4** illustrating the nature of the singlet excited state in the emission band in the region 340–380 nm. For each state the transition energy (eV) and the oscillator strength (in parentheses) are listed. Shown are only occupied (holes) and unoccupied (electrons) NTO pairs that contribute more than 30% to each excited state.

combination of $\pi(\text{Ph})$ with $p(\text{coligand})$ in chloro and bromo complexes whereas different amounts of metal-d participation is found in acetato and iodo analogues. The NTO analysis, therefore, suggest a ligand-dominated emissive states $\pi^*(\text{azo} + \text{Ph})$ by virtue of their enhanced stability. The structurally similar luminescence spectra can be assigned as intraligand $\pi\text{-}\pi^*$ transitions within the planar bisazo chromophore perturbed by the anionic coligands and metal in varying extent. Notably, no metal contribution ($d_{x^2-y^2}$) was found computationally in the emissive state of the present palladacycles. It should be noted that the reports of luminescent of azo complexes are less documented in the literature.²⁰

Catalysis

Many of the N-donor ligands are inexpensive and stable in air unlike phosphine ligands. Facile synthesis, stability and easy handling of non-phosphine cyclometalated Pd complexes are accountable for their popularity and growing applications in catalysis. Since the C–C coupling reactions are of vital importance in organic synthesis and the palladacycles are a class of typical catalysts in these reactions,^{12a,15d,e,1} the Suzuki–Miyaura cross-coupling reaction of aryl halides with phenylboronic acid was carried out to explore the catalytic activity of the non-phosphine pincers **1** and **4**. Upon heating a mixture of phenylbromide, phenylboronic acid and K_2CO_3 in toluene at 70 °C for 3 h in the presence of Pd complexes, the biaryls were isolated in excellent yields for aryl bromides (Table 4). In general, the

Table 4 Suzuki–Miyaura Coupling Reaction of **1** and **4** with Aryl halides and Phenylboronic Acid^a



Entry	Catalyst	R	X	Amount of cat. (mol%)	T (°C)	t (h)	Product	Yield (%) ^b	TON ^c
1	1	COCH ₃	Br	0.001	70	3	5	83	83000
2	4	COCH ₃	Br	0.001	70	3	5	81	81000
3	1	NO ₂	Br	0.001	70	3	6	89	89000
4	4	NO ₂	Br	0.001	70	3	6	88	88000
5	1	CN	Br	0.001	70	3	7	93	93000
6	4	CN	Br	0.001	70	3	7	92	92000
7	1	COCH ₃	Cl	0.01	110	6	5	10	1000

8	1	NO ₂	Cl	0.01	110	6	6	63	6300
9	1	CN	Cl	0.01	110	6	7	60	6000

^a Reaction conditions: aryl halide (1.0 mmol), phenyl boronic acid (1.3 mmol), K₂CO₃ (2 mmol), Pd catalyst, toluene (5 mL). ^b isolated yield. ^c TON, turnover number {(mol of product)/(mol of catalyst)}.

electron rich palladium center is beneficial toward Suzuki-Miyaura coupling reactions. The reported electron deficient palladacycles **1** and **4** show high turnover numbers with good yields for certain substituted bromobenzenes. As shown in Table 4, only the strong electron-withdrawing group on phenyl bromides can generate the corresponding products. Notably, we were unable to isolate any coupling product upon varying the substituents on phenylbromides from strong electron-withdrawing to moderate electron-withdrawing groups *e.g.*, carbaldehyde or electron-donating groups *e.g.*, methoxy derivative under similar reaction conditions. To explore the versatility of the reported palladacycles, the coupling between aryl chlorides and phenyl boronic acid had also been performed. Aryl chlorides provide the corresponding biaryls in moderate to low yields (entries 7–9) with 0.01 mol % catalyst loading. Examples of Suzuki-Miyaura coupling using aryl chlorides are scarce with CN₂ coordinated pincer palladacycles.^{15d}

The report of the C–C cross coupling by Heck-type reactions catalyzed by the non-NHC *CNN* pincer Palladacycles are sparsely known.^{12e,g,h} The high stability of the present pincer complexes may make themselves as promising candidates to achieve the high turnover numbers (TON's) under the harsh conditions of the Heck coupling reactions. In this context, preliminary investigations into the ability of easily accessible complexes **1** and **4** to act as precatalysts have been tested for Heck-type coupling reactions. The results obtained are summarized in Table 5. Though catalysis was observed in both the cases, the acetato complex **1** shows somewhat better activity compared to that of the iodo analogue **4**. All the reactions have been performed under argon with 0.01 mol% of catalysts in DMF at 135 °C with

Table 5 Heck Coupling of **1** and **4** with Functionalized Aryl Halides and Styrene^a

Entry	Catalyst	R	X	Amount of cat. (mol%)	Product	Yield (%) ^b	TON ^c
1	1	H	I	0.01	8	74	7400
2	4	H	I	0.01	8	70	7000
3	1	CHO	Br	0.01	9	84	8400
4	4	CHO	Br	0.01	9	86	8600
5	4	CHO	Br	0.001	9	83	83000
6	1	COCH ₃	Br	0.01	10	72	7200
7	4	COCH ₃	Br	0.01	10	68	6800
8	1	NO ₂	Br	0.01	11	79	7900

9	4	NO ₂	Br	0.01	11	76	7600
10	1	OCH ₃	Br	0.01	12	63	6300
11	4	OCH ₃	Br	0.01	12	58	5800

^a Reaction conditions: aryl halide (1.0 mmol), styrene (1.5 mmol), K₂CO₃ (1.8 mmol), Pd catalyst, dimethylformamide (7 mL), 135°C, 18 h. ^b isolated yield. ^c TON, turnover number {(mol of product)/(mol of catalyst)}.

K₂CO₃ (1.8 equiv. of base). The use of 0.001 mol % catalyst loading merely affects the efficiency (entry 5). The complexes under investigation are thermally stable and inert toward air and moisture in the solid state. These properties allowed for catalytic experiments under aerobic conditions as well. The use of K₂CO₃ as base furnished better yield compared to that of NaOAc for the coupling reactions. Different *para*-functionalized aryl halides are used in the catalytic experiments. The palladacycles have shown good catalytic activity over 18 h at elevated temperature with activated substrates such as 4-bromobenzaldehyde, 4-bromonitrobenzene and 4-bromoacetophenone. A slightly lower activity was observed with the deactivated substrates like 4-bromoanisole. The coupling of bromobenzene with styrene proceeded also with low yield.

Conclusion

We have introduced a typical bisazobenzene, 2-(phenylazo)azobenzene, as the novel chelating ligand and have presented a high-yield preparation of a new class of unsymmetrical C_{Ph}N_{azo}N_{azo} pincer palladacycles with the symmetrical ligand. The reported palladacycles represent the first member of pincer compounds containing two N_{azo} atoms. A noteworthy feature of the ligand is the presence of two conjugated π -acidic azo chromophores, which makes it both a superior σ -donor as well as π -acceptor relative to azobenzene. Remarkable stabilization of azo-based virtual orbitals is also apparent upon palladation, where LC (LUMO and LUMO + 1) states are computed to be the lower energy orbitals relative to MC (LUMO + 2) level. Low-lying nature of LUMO and LUMO +1 in the free ligand as well as in all the palladacycles is nicely substantiated with the electrochemical study. In consequence, modification of FMOs leads to interesting optoelectronic property in the palladacycles. The cyclopalladated compounds exhibit luminescence in solution at room temperature. This property is plausibly as a result of the enhanced stability of LC emissive states (azo π^*) which are hardly mixed by non-emissive state ($d_{x^2-y^2}$). The similarity in luminescence spectra of the cyclometalated complexes suggest a ligand-dominated emissive state, which can be assigned essentially as intraligand π - π^* transitions admixed with little coligands and/or metal orbitals. Among the palladacycles, the iodo complex exhibits the longest wave-length visible transition near 600 nm. The observed bathochromic shift of the lowest energy transition in chloro to iodo compounds is caused by the incorporation of $\pi(\text{halide}) \rightarrow \pi^*(\text{PAAB})$ LLCT character to a greater extent, consistent with the polarizability order of the halides. In contrast, analogous excitation in the chloro and acetato derivatives is dominated by $4d_{zx}(\text{Pd}) \rightarrow \pi^*(\text{PAAB})$ MLCT. The transitions in the UV

region are almost entirely bisazoaromatic-based π - π^* admixed with little participation of metal or coligand orbitals. In addition, the results of C–C cross-coupling reactions show that the *CNN* palladacycles may be employed in the advancement of effective catalysts for Suzuki-Miyaura and Heck-type reactions. Novel functionalized bisazoaromatic ligands and their cyclometalated complexes are currently under investigation.

Experimental Section

General Information

All manipulations were performed under an atmosphere of argon except where mentioned. Solvents were dried by standard methods and distilled under argon prior to use. Palladium chloride, palladium acetate and styrene were purchased from Aldrich Chemical Company. Other chemicals and solvents were purchased from Merck, India and dried before use according to standard methods.

Synthesis of Ligand

2-(phenylazo)azobenzene (PAAB). 2-amino-azobenzene²¹ (5 g, 0.025 mol) was dissolved in 20 mL glacial acetic acid with heating. Solid nitrosobenzene (2.9 g, 0.027 mol) was added and the mixture was stirred for 24 h at 50 °C until the precipitation of a dark mass was obtained. The precipitate was dried in vacuo and subsequently dissolved in minimum volume of hot *n*-hexane. The deep red crystals were obtained from the hot hexane solution. An *n*-hexane extract was made with the filtrate, giving an additional crop of red crystals. Yield: 6.24 g, 86%. mp. 107–108 °C (lit. mp. 106–108 °C);¹¹ FT-IR (cm^{-1}): 1486-1439 ($\nu_{\text{N=N}}$); ¹H NMR (300 MHz, CDCl_3): δ 7.96-7.98 (m, 4H), 7.76 (q, 2H, $J = 3.3$ Hz), 7.51–7.58 (m, 8H). ¹³C NMR (300 MHz, CDCl_3): δ 153.1, 148.2, 139.3, 130.9, 129.1, 123.3, 118.2. Elem. Anal. Calcd (%) for $\text{C}_{18}\text{H}_{14}\text{N}_4$: C, 75.50; H, 4.93; N, 19.57. Found: C, 75.44; H, 4.87; N, 19.42. HRMS (ESI): m/z calcd. for $\text{C}_{18}\text{H}_{15}\text{N}_4$ 287.1297; found 287.1293 ($\text{M} + \text{H}$)⁺.

Synthesis of Complexes

[Pd(L)(OAc)] 1. To a solution of PAAB (317 mg, 1.1 mmol) in AcOH (25 mL) was added $\text{Pd}(\text{OAc})_2$ (226 mg, 1.0 mmol) under an argon atmosphere. The mixture was stirred at room temperature for 80 h. The solvent was removed under reduced pressure. Crystallization by slow diffusion of toluene solution of the complex into hexane afforded **1** as rod shaped crystals (445 mg, 98% yield). FT-IR (cm^{-1}): 1446, 1430 ($\nu_{\text{N=N}}$), 3524 ($\nu_{\text{O-H}}$). ¹H NMR (300 MHz, CDCl_3): δ 8.31 (d, 1H, $J = 7.9$ Hz), 8.10 (d, 1H, $J = 6.0$ Hz), 7.95 (d, 1H, $J = 6.1$ Hz), 7.82 (d, 1H, $J = 7.0$ Hz), 7.76–7.67 (m, 5H), 7.56 (d, 3H, $J = 6.6$ Hz), 7.28 (s, 1H), 1.72 (s, 3H). ¹³C NMR (300 MHz, CDCl_3): δ 177.1, 165.6, 154.9, 152.3, 151.5, 134.3, 133.3, 132.1, 129.1, 128.7, 128.3, 126.9, 122.4, 117.9, 23.4. Elem. Anal. Calcd (%) for $\text{C}_{20}\text{H}_{16}\text{N}_4\text{O}_2\text{Pd}$: C, 53.29;

H, 3.58; N, 12.43. Found: C, 53.21; H, 3.62; N, 12.36. HRMS (ESI): m/z calcd. for $C_{18}H_{13}N_4Pd$ 391.0182; found 391.0180 ($M - OAc$)⁺.

[Pd(L)Cl] 2. To a solution of PAAB (193 mg, 0.674 mmol) in EtOH (25mL) was added $K_2[PdCl_4]$ (200 mg, 0.612 mmol) under an argon atmosphere. The mixture was stirred at room temperature for 80 h, until a dark red solution was formed. The solvent was removed under reduced pressure. Crystallization by slow diffusion of toluene solution of the complex into hexane afforded **2** as rod shaped crystals (251 mg, 96% yield). FT-IR (cm^{-1}): 1446, 1430 ($\nu_{N=N}$). 1H NMR (300 MHz, $CDCl_3$): δ 8.32 (d, 1H, $J = 7.0$ Hz), 8.11 (d, 1H, $J = 6.9$ Hz), 7.97 (d, 1H, $J = 5.8$ Hz), 7.83 (d, 1H, $J = 7.0$ Hz), 7.77–7.68 (m, 5H), 7.57 (d, 3H, $J = 7.2$ Hz), 7.29 (s, 1H). ^{13}C NMR (300 MHz, $CDCl_3$): δ 165.9, 152.7, 137.1, 133.7, 133.4, 132.6, 129.4, 128.7, 123.1, 118.4. Elem. Anal. Calcd. (%) for $C_{18}H_{13}N_4ClPd$: C, 50.61; H, 3.07; N, 13.12. Found: C, 50.53; H, 3.18; N, 12.97. HRMS (ESI): m/z for $C_{18}H_{13}N_4Pd$ 391.0182; found 391.0188 ($M - Cl$)⁺, calcd 819.0052; found 819.0059 ($2M - Cl$)⁺.

[Pd(L)Br] 3. To a solution of **1** (200 mg, 0.444 mmol) in acetone, KBr solution (10^{-2} molar solution in water) was added dropwise and the resulting solution was stirred for 1 h at room temperature. The dark residue was filtered and dried in vacuum (191 mg, 91% yield). FT-IR (cm^{-1}): 1444, 1430 ($\nu_{N=N}$). 1H NMR (300 MHz, $CDCl_3$): δ 8.31 (d, 1H, $J = 6.9$ Hz), 8.11 (d, 1H, $J = 6.2$ Hz), 7.95 (d, 1H, $J = 5.6$ Hz), 7.82 (d, 1H, $J = 6.9$ Hz), 7.76–7.68 (m, 5H), 7.56 (d, 3H, $J = 7.5$ Hz), 7.28 (s, 1H). ^{13}C NMR (300 MHz, $CDCl_3$): δ 162.3, 139.5, 133.7, 133.6, 133.4, 132.5, 129.5, 128.8, 126.8, 123.0, 118.5. Elem. Anal. Calcd. (%) for $C_{18}H_{13}N_4BrPd$: C, 45.84; H, 2.78; N, 11.88. Found: C, 45.71; H, 2.61; N, 11.75. HRMS (ESI): m/z for $C_{18}H_{13}N_4Pd$ 391.0182; found 391.0186 ($M - Br$)⁺, calcd 862.9543; found 862.9547 ($2M - Br$)⁺.

[Pd(L)I] 4. The complex **4** was prepared from **1** (200 mg, 0.444 mmol) with KI using similar procedure applied for the synthesis of complex **3** (212 mg, 92% yield). FT-IR (cm^{-1}): 1435, 1383 ($\nu_{N=N}$). 1H NMR (300 MHz, $CDCl_3$): 8.48 (d, 1H, $J = 7.7$ Hz), 8.36 (d, 1H, $J = 7.3$ Hz), 8.16 (d, 1H, $J = 8.9$ Hz), 8.01 (d, 1H, $J = 7.4$ Hz), 7.73–7.67 (m, 5H), 7.56 (d, 3H, $J = 7.5$ Hz), 7.22 (s, 1H). ^{13}C NMR (300 MHz, $CDCl_3$): δ 166.4, 144.0, 133.9, 133.8, 133.5, 132.6, 129.8, 129.0, 126.6, 123.2, 118.7. Elem. Anal. Calcd. (%) for $C_{18}H_{13}N_4IPd$: C, 41.68; H, 2.53; N, 10.80. Found: C, 41.49; H, 2.39; N, 10.65. HRMS (ESI): m/z for $C_{18}H_{13}N_4Pd$ 391.0182; found 391.0181 ($M - I$)⁺, calcd 910.9414; found 910.9412 ($2M - I$)⁺.

General procedure for Suzuki–Miyaura Coupling reactions

A mixture of K_2CO_3 (2 mmol), aryl halide (1 mol) and phenyl boronic acid (1.3 mmol) were added in a flask and put under an atmosphere of argon followed by addition of 5 mL degassed toluene. After thermostating at an indicated temperature (typically at 70 °C) for 15 min, the catalyst was added against a positive stream of argon. The mixture was allowed to heat with stirring for the requisite time. After

cooling to ambient temperature, the solvent was removed under vacuum and purified by column chromatography on silica gel, using 20:1 hexane/ethyl acetate as eluent. Products were identified by comparison of NMR data with those in the literature.

4-Acetylbiphenyl (5).^{22a} ¹H NMR: (300 MHz, CDCl₃): δ 8.06 (d, *J* = 8.4 Hz, 2H), 7.71 (d, *J* = 8.7 Hz, 2H), 7.66 (d, *J* = 8.4 Hz, 2H), 7.53-7.42 (m, 3H), 2.66 (s, 3H). ¹³C NMR (300 MHz, CDCl₃): δ 197.7, 145.8, 139.9, 135.9, 131.9, 129.9, 128.9, 128.2, 127.2, 26.6.

4-Nitro-biphenyl (6).^{22a} ¹H NMR (300 MHz, CDCl₃): δ 8.23 (d, *J* = 8.7 Hz, 2H), 7.76 (d, *J* = 8.4 Hz, 2H), 7.66 (d, *J* = 8.4 Hz, 2H), 7.47-7.55 (m, 3H). ¹³C NMR (300 MHz, CDCl₃): δ 147.6, 147.1, 138.7, 129.2, 128.9, 127.8, 127.4, 124.1.

4-Phenylbenzotrile (7).^{22b} ¹H NMR (300 MHz, CDCl₃): δ 7.72 (d, *J* = 8.4 Hz, 2H), 7.66 (d, *J* = 7.5 Hz, 2H), 7.59 (d, *J* = 8.1 Hz, 2H), 7.53—7.42 (m, 3H). ¹³C NMR (300 MHz, CDCl₃): δ 145.6, 139.2, 132.6, 129.1, 128.7, 127.7, 127.2, 118.9, 110.9.

General procedure for Heck-coupling reactions

A mixture of K₂CO₃ (1.8 mmol), aryl halide (1 mmol) and styrene (1.5 mmol) were added in a flask and put under an atmosphere of argon followed by addition of 7 mL degassed DMF. After thermostating at 135 °C for 15 min the catalyst (0.01 mol%) was added against a positive stream of argon. The mixture was allowed to heat at 135 °C for 18 h. After cooling to ambient temperature, the solvent was removed under vacuum and purified by column chromatography on silica gel, using 20:1 hexane/ethyl acetate as eluent. Products were identified by comparison of NMR data with those in the literature.

(E)-1,2-Diphenylethene (8).^{22a} ¹H NMR (400 MHz, CDCl₃): δ 7.51 (d, 4H, *J* = 7.6 Hz), 7.36 (t, 4H, *J* = 8.0 Hz), 7.26 (t, 2H, *J* = 7.2 Hz), 7.11 (s, 2H). ¹³C NMR (300 MHz, CDCl₃): δ 137.4, 128.8, 127.9, 127.7, 126.6.

(E)-1-Formyl-4-styrylbenzene (9).^{22a} ¹H NMR (400 MHz, CDCl₃): δ 9.99 (s, 1H), 7.87 (d, 2H, *J* = 8.4 Hz), 7.66 (d, 2H, *J* = 8.4 Hz), 7.55 (d, 2H, *J* = 7.6 Hz), 7.39 (t, 2H, *J* = 8.0 Hz), 7.32 (t, 1H, *J* = 7.2 Hz), 7.27 (d, 1H, *J* = 16.4 Hz), 7.15 (d, 1H, *J* = 16.4 Hz). ¹³C NMR (300 MHz, CDCl₃): δ 191.6, 143.4, 136.6, 135.4, 132.2, 130.2, 128.8, 128.5, 127.3, 126.9.

(E)-1-Acetyl-4-Styrylbenzene (10).^{22a} ¹H NMR (400 MHz, CDCl₃): δ 7.96 (d, 2H, *J* = 8.4 Hz), 7.59 (d, 2H, *J* = 8.4 Hz), 7.55 (d, 2H, *J* = 7.2 Hz), 7.39 (t, 2H, *J* = 8.0 Hz), 7.30 (t, 1H, *J* = 7.2 Hz), 7.24 (d, 1H, *J* = 17.2 Hz), 7.14 (d, 1H, *J* = 16.4 Hz), 2.62 (s, 3H). ¹³C NMR (300 MHz, CDCl₃): δ 197.5, 142.0, 136.7, 136.0, 131.5, 128.9, 128.8, 128.3, 127.5, 126.8, 126.5, 26.6.

(E)-1-Nitro-4-styrylbenzene (11).^{22a} ¹H NMR (300 MHz, CDCl₃): δ 8.22 (d, 2H, *J* = 8.7 Hz), 7.64 (d, 2H, *J* = 8.7 Hz), 7.55 (d, 2H, *J* = 7.1 Hz), 7.42-7.33 (m, 3H), 7.28 (d, 1H, *J* = 16.3 Hz), 7.14 (d, 1H, *J* = 16.5 Hz). ¹³C NMR (300 MHz, CDCl₃): δ 146.8, 143.9, 136.2, 133.3, 128.9, 128.8, 127.0, 126.9, 126.3, 124.1.

(E)-1-Methoxy-4-styrylbenzene (12).^{22a} ¹H NMR (400 MHz, CDCl₃): δ 7.49 (d, 2H, $J = 7.6$ Hz), 7.46 (d, 2H, $J = 8.4$ Hz), 7.35 (t, 2H, $J = 7.6$ Hz), 7.23 (t, 1H, $J = 7.2$ Hz), 7.07 (d, 1H, $J = 16$ Hz), 6.97 (d, 1H, $J = 16.4$ Hz), 6.90 (d, 2H, $J = 8.8$ Hz), 3.83 (s, 3H). ¹³C NMR (300 MHz, CDCl₃): δ 159.4, 137.7, 130.2, 128.7, 128.3, 127.7, 127.2, 126.7, 126.3, 114.2, 55.3.

Physical Measurements

The elemental analyses (C, H, N) were performed with a Perkin-Elmer model 2400 series II elemental analyzer. FT-IR spectra were recorded on Perkin-Elmer L1600300 spectrometer. The attenuated total reflectance method was used. NMR spectral measurement was carried out on Bruker FT 300 MHz and Bruker DPX-400 MHz spectrometers with TMS as an internal reference. The electrospray ionization mass spectra (ESI-MS positive) were measured in acetonitrile on Waters HRMS spectrometers (Model: QTOF Micro YA263). Thermogravimetric analysis (TGA) was carried out using a SDT Q600 V8.2 Built 100 thermal analyzer. The electronic spectra in dichloromethane solution were obtained using a Perkin-Elmer LAMDA 25 spectrophotometer with a solute concentration of about 10^{-4} M. Emission spectra were recorded on PTI QM40 spectrometer in deaerated dichloromethane solutions at room temperature. Emission quantum yields of the complexes were determined in deaerated solutions of the complexes by a relative method using anthracene in ethanol as the standard.²³ The emission quantum yield (Φ_r) and radiative (k_r) and nonradiative (k_{nr}) decay rate constants for complexes was calculated by the equations²⁴ given below:

$$\Phi_r = \Phi_{\text{std}} \frac{A_{\text{std}}}{A_r} \frac{I_r}{I_{\text{std}}} \frac{\eta_r^2}{\eta_{\text{std}}^2} \quad (3)$$

$$k_r = \frac{\Phi}{\tau} \quad (4)$$

$$k_{nr} = \frac{1 - \Phi}{\tau} \quad (5)$$

where Φ_r and Φ_{std} are the quantum yields of unknown and standard samples ($\Phi_{\text{std}}=0.27$ (at 298 K) in ethanol at $\lambda_{\text{ex}} = 341$ nm)²⁵, A_r and A_{std} (< 0.1) are the solution absorbances at the excitation wavelength (λ_{ex}), I_r and I_{std} are the integrated emission intensities, and η_r and η_{std} are the refractive indices of the solvents.²⁶ For all measurements, the same slit widths for excitation and emission were maintained. Time-correlated single photon counting (TCSPC) measurements were carried out for recording of the luminescence decay profile for the free ligand and Pd(II) complexes in dichloromethane solution using a picosecond diode laser (IBH Nanoled-07) in an IBH Fluorocube apparatus. Air-equilibrated solutions were used for recording of the luminescence lifetime. The fluorescence decays were collected on a Hamamatsu MCP photomultiplier (R3809). The fluorescence decays were analyzed using IBH DAS6 software. Electrochemical measurements were carried out at 27 °C with VersaStat II Princeton Applied

Research potentiostat/galvanostat under argon atmosphere. The cell contained a Pt working electrode and a Pt wire auxiliary electrode. Tetraethylammonium perchlorate (NEt_4ClO_4) was used as a supporting electrolyte and the potentials are referenced to the Ag/AgCl electrode without junction correction.

Crystallographic Studies

X-ray intensity data for all the compounds were measured at 296(2) K on Bruker AXS SMART APEX II equipped with a CCD diffractometer using graphite-monochromator ($\text{Mo K}\alpha$, $\lambda = 0.71073 \text{ \AA}$). Metal atoms were located by direct methods, and the rest of the non-hydrogen atoms emerged from successive Fourier synthesis. The structures were refined by full-matrix least squares procedures on F^2 . All the H atoms were included in calculated positions and treated as riding atoms using SHELXL default parameters (except those of water molecule in **1** which were found and isotopically refined). Calculations were performed using the SHELXTL v 6.14 program package.²⁷ Thermal ellipsoids are drawn at the 30% probability level. Molecular structure plots were drawn using the Oak Ridge thermal ellipsoid plot ORTEP.²⁸

Computational Study

The molecular geometry of the singlet ground state (S_0) of PAAB, **1**, **2**, **3** and **4** have been calculated by DFT method using the (R)B3LYP²⁹ hybrid functional approach incorporated in GAUSSIAN 09 program package.³⁰ The geometries of the complexes were fully optimized in gas phase without imposing any symmetry constraints. The nature of all the stationary points was checked by computing vibration frequencies, and all the species were found to be true potential energy minima, as no imaginary frequency were obtained ($\text{NImag} = 0$). The single crystal X-ray coordinates have been used as the initial input in all calculations. On the basis of the optimized geometries, the absorption and emission spectra properties in dichloromethane (CH_2Cl_2) media were calculated by the time-dependent density functional theory (TD-DFT)³¹ approach associated with the conductor-like polarizable continuum model (CPCM).³² We computed the lowest 100 singlet–singlet transitions in absorption and emission processes respectively. The electronic structure contributions to the differences in observed optoelectronic properties are compared by natural transition orbital (NTO) analysis. The computed vertical transitions were calculated at the equilibrium geometry of the S_0 state and described in terms of one-electron excitations of molecular orbitals of the corresponding S_0 geometry. The calculated transitions with moderate intensities ($f \geq 0.02$) can be envisaged going from the lower to the higher energy region of the spectrum. The palladium atom and iodine were described by a double- ζ basis set with the effective core potential of Hay and Wadt (LANL2DZ)³³ and the 6-311+G(d,p) basis set³⁴ was used for the other elements present in the complexes to optimize the ground state geometries. The calculated electronic density plots for frontier molecular

orbitals were prepared by using the GaussView 5.0 software. GaussSum program, version 2.2³⁵ was used to calculate the molecular orbital contributions from groups or atoms.

Acknowledgments

We thank the Department of Science and Technology, New Delhi, for financial assistance (grant SR/S1/IC-75/2010). We are also thankful to the Department of Science and Technology, New Delhi, India for the data collection on the CCD facility setup (Jadavpur University). We also acknowledge CAS, Department of Chemistry, Jadavpur University and the DST-PURSE program for other facilities. Thanks to Dr. S. Chakrabarti of University of Calcutta, Kolkata for computational assistance. Ms. S. Roy thanks DST and Mr. S. Pramanik and Mr. T. Ghorui thank UGC, New Delhi for the research fellowship.

Supporting Information Available

†Electronic supplementary information (ESI) available: NMR, absorption, emission spectra and photoluminescence decay of ligand, Tables and Figures for TD-DFT of complexes, crystallographic data and structure refinement parameters, coordinates of optimized geometries of complexes. CCDC 1031475–1031479. For ESI and crystallographic data in CIF or other electronic format see DOI:

References

1. A. C. Cope and R. W. Siekman, *J. Am. Chem. Soc.*, 1965, **87**, 3272–3273.
2. (a) A. Fernández, M. López-Torres, J. J. Fernández, D. Vázquez-García and J. M. Vila, *J. Chem. Educ.*, 2012, **89**, 156–158; (b) J.-P. Djukic, A. Hijazi, H. D. Flack and G. Bernardinelli, *Chem. Soc. Rev.*, 2008, **37**, 406–425; (c) J. Dupont and M. Pfeffer, *Palladacycles: Synthesis, Characterization and Applications*, Wiley-VCH Verlag GmbH & Co, 2008; (d) M. Ghedini, I. Aiello, A. Crispini, A. Golemme, M. L. Deda and D. Pucci, *Coord. Chem. Rev.*, 2006, **250**, 1373–1390; (e) M. Albrecht, *Chem. Rev.*, 2010, **110**, 576–623; (f) V. V. Dunina, O. A. Zalevskaya and V. M. Potapov, *Russ. Chem. Rev.*, 1988, **57**, 250–269.
3. (a) N. Deibel, M. G. Sommer, S. Hohloch, J. Schwann, D. Schweinfurth, F. Ehret and B. Sarkar, *Organometallics*, 2014, **33**, 4756–4765; (b) O. A. Blackburn and B. J. Coe, *Organometallics*, 2011, **30**, 2212–2222; (c) A. R. Dick, M. S. Remy, J. W. Kampf and M. S. Sanford, *Organometallics*, 2007, **26**, 1365–1370; (d) I. Omae, *Coord. Chem. Rev.*, 2004, **248**, 995–1023; (e) M. Ghedini, D. Pucci, A. Crispini, G. Barberio, I. Aiello, F. Barigelletti, A. Gessi and O. Francescangeli, *Appl. Organomet. Chem.*, 1999, **13**, 565–581; (f) C. Sinha, D. Bandyopadhyay and A. Chakravorty, *Inorg. Chem.*, 1988, **27**, 1173–1178; (g) A. K. Mahapatra, D. Bandyopadhyay, P. Bandyopadhyay and A. Chakravorty, *Inorg. Chem.*, 1986, **25**, 2214–2221; (h) A. D. Ryabov, *Synthesis*, 1985, 233–252; (i) I. Omae, *Chem. Rev.*,

1979, **79**, 287–321; (j) M. I. Bruce, B. Goodall and G. A. Stone, *J. Chem. Soc., Dalton Trans.*, 1978, 687–694; (k) M. I. Bruce, *Angew. Chem., Int. Ed.* 1977, **16**, 73–86; (l) J. Dehand and M. Pfeffer, *Coord. Chem. Rev.*, 1976, **18**, 327–352; (m) G. W. Parshall, *Acc. Chem. Res.*, 1970, **3**, 139–144; (n) H. Takahashi and J. Tsuji, *J. Organomet. Chem.*, 1967, **10**, 511–517.

4. (a) M. Juribašić, K. Užarević, D. Gracin and M. Ćurić, *Chem. Commun.*, 2014, **50**, 10287–10290; (b) M. Juribašić, I. Halasz, D. Babić, D. Cinčić, J. Plavec and M. Ćurić, *Organometallics*, 2014, **33**, 1227–1234; (c) M. Juribašić, A. Budimir, S. Kazazić and M. Ćurić, *Inorg. Chem.*, 2013, **52**, 12749–12757; (d) N. Deibel, S. Hohloch, M. G. Sommer, D. Schweinfurth, F. Ehret, P. Braunstein and B. Sarkar, *Organometallics*, 2013, **32**, 7366–7375 and references therein; (e) D. Cinčić, M. Juribašić, D. Babić, K. Molčanov, P. Šket, J. Plavec and M. Ćurić, *Chem. Commun.*, 2011, **47**, 11543–11545; (f) D. Babić, M. Ćurić, K. Molčanov, G. Ilc and J. Plavec, *Inorg. Chem.*, 2008, **47**, 10446–10454; (g) M. Ćurić, D. Babić, A. Višnjevac and K. Molčanov, *Inorg. Chem.*, 2005, **44**, 5975–5977.

5. O. A. Blackburn, B. J. Coe and M. Helliwell, *Organometallics*, 2011, **30**, 4910–4923.

6. (a) I. Chakraborty, S. J. Carrington and P. K. Mascharak, *Acc. Chem. Res.*, 2014, **47**, 2603–2611; (b) M. Han, T. Hiradeb and Y. Okuib, *Dalton Trans.*, 2014, **43**, 5929–5934; (c) T. Hirade, Y. Okui and M. Han, *J. Mater. Chem. C*, 2013, **1**, 2672–2679; (d) M. E. Moustafa, M. S. McCready and R. J. Puddephatt, *Organometallics*, 2012, **31**, 6262–6269; (e) O. A. Blackburn, B. J. Coe, J. Fielden, M. Helliwell, J. J. W. McDouall and M. G. Hutchings, *Inorg. Chem.*, 2010, **49**, 9136–9150; (f) M. J. Baena, P. Espinet, C. L. Folcia, J. Ortega and J. Etxebarri, *Inorg. Chem.*, 2010, **49**, 8904–8913; (g) M. Juribašić, M. Ćurić, K. Molčanov, D. Matković-Čalogović and D. Babić, *Dalton Trans.*, 2010, **39**, 8769–8778; (h) M. Han, T. Hirade and M. Hara, *New J. Chem.*, 2010, **34**, 2887–2891; (i) P. Pratihar, T. K. Mondal, A. K. Patra and C. Sinha, *Inorg. Chem.*, 2009, **48**, 2760–2769; (j) M. Ghedini, I. Aiello, A. Crispini, A. Golemme, M. La Deda and D. Pucci, *Coord. Chem. Rev.*, 2006, **250**, 1373–1390.

7. Room temperature luminescent palladacycles in solution: (a) P.-K. Chow, W.-P. To, K.-H. Low and C.-M. Che, *Chem. Asian J.*, 2014, **9**, 534–545; (b) S. Lentijo, J. A. Miguel and P. Espinet, *Organometallics*, 2011, **30**, 1059–1066; (c) S. M. Borisov, G. Zenkl and I. Klimant, *ACS Appl. Mater. Interfaces*, 2010, **2**, 366–374; (d) C. Bronner, S. A. Baudron, M. W. Hosseini, C. A. Strassert, A. Guenet and L. De Cola, *Dalton Trans.*, 2010, **39**, 180–184; (e) M. La Deda, M. Ghedini, I. Aiello, T. Pugliese, F. Barigelletti and G. Accorsi, *J. Organomet. Chem.*, 2005, **690**, 857–861; (f) C. S. Consorti, G. Ebeling, F. Rodembusch, V. Stefani, P. R. Livotto, F. Rominger, F. H. Quina, C. Yihwa and J. Dupont, *Inorg. Chem.*, 2004, **43**, 530–536; (g) M. Ghedini, I. Aiello, M. La Deda and A. Grisolia, *Chem. Commun.*, 2003, 2198–2199; (h) Y. Wakatsuki, H. Yamazaki, P. A. Grutsch, M. Santhanam and C. Kotal, *J. Am. Chem. Soc.*, 1985, **107**, 8153–8159.

8. Room temperature luminescent palladacycles in solid: (a) D. V. Aleksanyan, V. A. Kozlov, Y. V. Nelyubina, K. A. Lyssenko, L. N. Puntus, E. I. Gutsul, N. E. Shepel, A. A. Vasil'ev, P. V. Petrovskii and

- I. L. Odinets, *Dalton Trans.*, 2011, **40**, 1535–1546; (b) J. Kuwabara, Y. Ogawa, A. Taketoshi and T. Kanbara, *J. Organomet. Chem.*, 2011, **696**, 1289–1293; (c) V. A. Kozlov, D. V. Aleksanyan, Y. V. Nelyubina, K. A. Lyssenko, E. I. Gutsul, L. N. Puntus, A. A. Vasil'ev, P. V. Petrovskii and I. L. Odinets, *Organometallics*, 2008, **27**, 4062–4070; (d) M. Akaiwa, T. Kanbara, H. Fukumoto and T. Yamamoto, *J. Organomet. Chem.*, 2005, **690**, 4192–4196; (e) F. Neve, A. Crispini, C. Di Pietro and S. Campagna, *Organometallics*, 2002, **21**, 3511–3518; (f) B.-C. Tzeng, S.-C. Chan, M. C. W. Chan, C.-M. Che, K.-K. Cheung and S.-M. Peng, *Inorg. Chem.*, 2001, **40**, 6699–6704; (g) F. Neve, A. Crispini and S. Campagna, *Inorg. Chem.*, 1997, **36**, 6150–6156.
9. P. K. Chow, C. Ma, W.-P. To, G. S. M. Tong, S.-L. Lai, S. C. F. Kui, W.-M. Kwok and C.-M. Che, *Angew. Chem., Int. Ed.*, 2013, **52**, 11775–11779.
10. (a) M. Maestri, V. Balzani, C. Deuschel-Cornioley and A. Von Zelewsky, ed. D. Volman, G. Hammond, and D. Neckers, *Advanced Photochemistry*, John Wiley & Sons, New York, 1992, pp. 1–68; (b) G. R. Crosby, *Acc. Chem. Res.*, 1975, **8**, 231–238.
11. P. Ruggli and J. Rohner, *Helv. Chim. Acta*, 1942, **25**, 1533–1542.
12. (a) T. Wang, X.-Q. Hao, J.-J. Huang, K. Wang, J.-F. Gong and M.-P. Song, *Organometallics*, 2014, **33**, 194–205; (b) K. M. Engle and J.-Q. Yu, *J. Org. Chem.*, 2013, **78**, 8927–8955. (c) A. Abellán-López, M. T. Chicote, D. Bautista and J. Vicente, *Organometallics*, 2012, **31**, 7434–7446; (d) D. Vázquez-García, A. Fernández, M. López-Torres, A. Rodríguez, A. Varela, M. T. Pereira, J. M. Vila and J. J. Fernández, *Organometallics*, 2011, **30**, 396–404; (e) T. Wang, X.-Q. Hao, J.-J. Huang, K. Wang, J.-F. Gong and M.-P. Song, *Dalton Trans.*, 2011, **40**, 8964–8976 (f) M. Bröring, C. Kleeberg and S. Köhler, *Inorg. Chem.*, 2008, **47**, 6404–6412; (g) B. L. Dietrich, J. Egbert, A. M. Morris and M. Wicholas, *Inorg. Chem.*, 2005, **44**, 6476–6481; (h) K.-M. Wu, C.-A. Huang, K.-F. Peng and C.-T. Chen *Tetrahedron*, 2005, **61**, 9679–9687; (i) C.-T. Chen, Y.-S. Chan, Y.-R. Tzeng and M.-T. Chen, *Dalton Trans.*, 2004, 2691–2696; (j) S.-W. Lai, T.-C. Cheung, M. C. W. Chan, K.-K. Cheung, S.-M. Peng and C.-M. Che, *Inorg. Chem.*, 2000, **39**, 255–262.
13. D. Morales-Morales and C. M. Jensen, *The Chemistry of Pincer Compounds*, Elsevier, Amsterdam, 2007.
14. (a) P. Ghosh, S. Samanta, S. K. Roy, S. Demeshko, F. Meyer and S. Goswami, *Inorg. Chem.*, 2014, **53**, 4678–4686; (b) P. Majumder, S. Baksi, S. Halder, H. Tadesse, A. J. Blake, M. G. B. Drew and S. Bhattacharya, *Dalton Trans.*, 2011, **40**, 5423–5425.
15. (a) X.-Q. Hao, Y.-W. Zhao, J.-J. Yang, J.-L. Niu, J.-F. Gong and M.-P. Song, *Organometallics*, 2014, **33**, 1801–1811; (b) G. R. Rosa and D. S. Rosa, *RSC Adv.*, 2012, **2**, 5080–5083; (c) X.-Q. Hao, Y.-X. Xu, M.-J. Yang, L. Wang, J.-L. Niu, J.-F. Gong and M.-P. Song *Organometallics* 2012, **31**, 835–846; (d) Q.-L. Luo, J.-P. Tan, Z.-F. Li, W.-H. Nan and D.-R. Xiao, *J. Org. Chem.*, 2012, **77**, 8332–8337; (e) K. Srinivas, P. Srinivas, P. S. Prathima, K. Balaswamy, B. Sridhar and M. M. Rao, *Catal. Sci. Technol.*,

- 2012, **2**, 1180–118; (f) N. Selander and K. J. Szabó, *Chem. Rev.*, 2011, **111**, 2048–2076; (g) V. A. Kozlov, D. V. Aleksanyan, Y. V. Nelyubina, K. A. Lyssenko, P. V. Petrovskii, A. A. Vasil'ev and I. L. Odinets, *Organometallics*, 2011, **30**, 2920–2932; (h) J.-L. Niu, X.-Q. Hao, J.-F. Gong and M.-P. Song, *Dalton Trans.*, 2011, **40**, 5135–5150; (i) R. Mosteiro, A. Fernández, D. Vázquez-García, M. López-Torres, A. Rodríguez-Castro, N. Gómez-Blanco, J. M. Vila and J. J. Fernández, *Eur. J. Inorg. Chem.*, 2011, 1824–1832; (j) L. Ray, M. M. Shaikh and P. Ghosh, *Organometallics*, 2007, **26**, 958–964; (k) J. Dupont, C. S. Consorti and J. Spencer, *Chem. Rev.*, 2005, **105**, 2527–2572; (l) I. P. Beletskaya and A. V. Cheprakov, *J. Organomet. Chem.*, 2004, **689**, 4055–4082; (m) M. Ćurić, D. Babić, Ž. Marinić, L. Paša-Tolić, V. Butković, J. Plavec and L. Tušek-Božić, *J. Organomet. Chem.*, 2003, **687**, 85–99.
16. (a) A. Kumar, G. K. Rao, S. Kumar and A. K. Singh, *Organometallics*, 2014, **33**, 2921–2943; (b) L. M. Mirica and J. R. Khusnutdinova, *Coord. Chem. Rev.*, 2013, **257**, 299–314; (c) A. de Meijere, F. Diederich, *Metal-Catalyzed Cross-coupling Reactions*; Wiley-VCH, New York, 2004.
17. C. Mills, *J. Chem. Soc.*, 1895, 925–933; (b) A. Baeyer, *Ber.*, 1874, **7**, 1638–1640.
18. (a) N. D. Paul, U. Rana, S. Goswami, T. K. Mondal and S. Goswami, *J. Am. Chem. Soc.*, 2012, **134**, 6520–6523; (b) W. Kaim, *Inorg. Chem.*, 2011, **50**, 9752–9765; (c) D. Das, T. K. Mondal, S. M. Mobin and G. K. Lahiri, *Inorg. Chem.*, 2009, **48**, 9800–9810; (d) K. Pramanik, M. Shivakumar, P. Ghosh and A. Chakravorty, *Inorg. Chem.*, 2000, **39**, 195–199.
19. R. L. Martin, *J. Chem. Phys.*, 2003, **118**, 4775–4777.
20. (a) S. Pramanik, S. Roy, T. Ghorui, S. Ganguly and K. Pramanik, *Dalton Trans.*, 2014, **43**, 5317–5334; (b) P. Mondal, A. Hens, S. Basak and K. K. Rajak, *Dalton Trans.*, 2013, **42**, 1536–1549; (c) L. Szabó, K. Herman, N. E. Mircescu, A. Fălămaș, L. F. Leopold, N. Leopold, C. Buzumurgă and V. Chiș, *Spectrochim. Acta, Part A*, 2012, **93**, 266–273; (d) K. Pramanik and B. Adhikari, *Polyhedron*, 2010, **29**, 1015–1022.
21. N. Maiti, S. Pal and S. Chattopadhyay, *Inorg. Chem.*, 2001, **40**, 2204–2205.
22. (a) G.-Q. Kong, S. Ou, C. Zou and C.-D. Wu, *J. Am. Chem. Soc.*, 2012, **134**, 19851–19857. (b) G. M. Scheuermann, L. Rumi, P. Steurer, W. Bannwarth, and R. Mülhaupt, *J. Am. Chem. Soc.*, 2009, **131**, 8262–8270.
23. B. P. Sullivan, D. J. Salmon, T. J. Meyer and J. Peedrin, *Inorg. Chem.*, 1979, **18**, 3369–3374.
24. J. V. Houten and R. J. Watts, *J. Am. Chem. Soc.*, 1976, **98**, 4853–4858.
25. (a) W. H. Melhuish, *J. Phys. chem.*, 1961, **65**, 229–235; (b) W. R. Dawson and M. W. Windsor, *J. Phys. Chem.*, 1968, **72**, 3251–3260 and references therein.
26. (a) F. I. El-Dossoki, *J. Chin. Chem. Soc.*, 2007, **54**, 1129–1137; (b) P. Pacak, *Chem. Papers.*, 1991, **45**, 227–232; (c) R. A. MacRae, E.T. Arakawa and M. W. Williams, *J. Chem. Eng. Data*, 1978, **23**, 189–190.
27. G. M. Sheldrick, SHELXTL Version 6.14, Bruker AXS Inc.: Madison, WI, 2003.

28. C. K. Johnson, *Report ORNL-5138*; Oak Ridge National Laboratory: Oak Ridge, TN, 1976.
29. (a) A. D. Becke, *J. Chem. Phys.*, 1993, **98**, 5648–5652; (b) C. Lee, W. Yang and R. G. Parr, *Phys. Rev. B*, 1988, **37**, 785–789.
30. M. J. Frisch, G. W. Trucks, H. B. Schlegel, G. E. Scuseria, M. A. Robb, J. R. Cheeseman, G. Scalmani, V. Barone, B. Mennucci, G. A. Petersson, H. Nakatsuji, M. Caricato, X. Li, H. P. Hratchian, A. F. Izmaylov, J. Bloino, G. Zheng, J. L. Sonnenberg, M. Hada, M. Ehara, K. Toyota, R. Fukuda, J. Hasegawa, M. Ishida, T. Nakajima, Y. Honda, O. Kitao, H. Nakai, T. Vreven, J. A. Montgomery Jr., J. E. Peralta, F. Ogliaro, M. Bearpark, J. J. Heyd, E. Brothers, K. N. Kudin, V. N. Staroverov, R. Kobayashi, J. Normand, K. Raghavachari, A. Rendell, J. C. Burant, S. S. Iyengar, J. Tomasi, M. Cossi, N. Rega, J. M. Millam, M. Klene, J. E. Knox, J. B. Cross, V. Bakken, C. Adamo, J. Jaramillo, R. Gomperts, R. E. Stratmann, O. Yazyev, A. J. Austin, R. Cammi, C. Pomelli, J. W. Ochterski, R. L. Martin, K. Morokuma, V. G. Zakrzewski, G. A. Voth, P. Salvador, J. J. Dannenberg, S. Dapprich, A. D. Daniels, O. Farkas, J. B. Foresman, J. V. Ortiz, J. Cioslowski and D. J. Fox, *Gaussian 09 Revision A.02*, Gaussian, Inc., Wallingford, CT, 2009.
31. (a) J. Autschbach, T. Ziegler, S. J. A. Gisbergen and E. J. Baerends, *J. Chem. Phys.*, 2002, **116**, 6930–6940; (b) K. L. Bak, P. Jørgensen, T. Helgaker, K. Rund and H. J. A Jensen, *J. Chem. Phys.*, 1993, **98**, 8873–8887; (c) T. Helgaker and P. Jørgensen, *J. Chem. Phys.*, 1991, **95**, 2595–2601; (d) E. K. U. Gross and W. Kohn, *Adv. Quantum Chem.*, 1990, **21**, 255–291.
32. (a) M. Cossi, N. Rega, G. Scalmani and V. Barone, *J. Comput. Chem.*, 2003, **24**, 669–681; (b) Cossi, M.; Barone, V. *J. Chem. Phys.*, 2001, **115**, 4708–4717; (c) V. Barone and M. Cossi, *J. Phys. Chem. A*, 1998, **102**, 1995–2001.
33. (a) P. J. Hay and W. R. Wadt, *J. Chem. Phys.*, **1985**, *82*, 299–310; (b) P. J. Hay and W. R. Wadt, *J. Chem. Phys.*, 1985, **82**, 270–283.
34. (a) M. S. Gordon, J. S. Binkley, J. A. Pople, W. J. Pietro and W. J. Hehre, *J. Am. Chem. Soc.*, 1982, **104**, 2797–2803; (b) J. S. Binkley, J. A. Pople and W. J. Hehre, *J. Am. Chem. Soc.*, 1980, **102**, 939–947.
35. N. M. O'Boyle, A. L. Tenderholt and K. M. Langner, *J. Comp. Chem.*, 2008, **29**, 839–845.